Journal of Magnetic Resonance 208 (2011) 4–19

Contents lists available at ScienceDirect

Journal of Magnetic Resonance

journal homepage: www.elsevier.com/locate/jmr

Structure of the two-dimensional relaxation spectra seen within the eigenmode perturbation theory and the two-site exchange model

Dimitri Bytchenkoff *, Stéphane Rodts *

Université Paris-Est, UMR Navier (LCPC-ENPC-CNRS), Champs sur Marne, France

ARTICLE INFO

Article history:
Received 10 May 2010
Revised 10 September 2010
Available online 1 October 2010

Keywords:
Diffusion
Relaxation
Porous
Laplace

ABSTRACT

The form of the two-dimensional (2D) NMR-relaxation spectra – which allow to study interstitial fluid dynamics in diffusive systems by correlating spin-lattice (T_1) and spin-spin (T_2) relaxation times – has given rise to numerous conjectures. Herein we find analytically a number of fundamental structural properties of the spectra: within the eigen-modes formalism, we establish relationships between the signs and intensities of the diagonal and cross-peaks in spectra obtained by various 1 and 2D NMR-relaxation techniques, reveal symmetries of the spectra and uncover interdependence between them. We investigate more specifically a practically important case of porous system that has sets of T_1- and T_2-eigenmodes and eigentimes similar to each other by applying the perturbation theory. Furthermore we provide a comparative analysis of the application of the, mathematically more rigorous, eigen-modes formalism and the, rather more phenomenological, first-order two-site exchange model to diffusive systems. Finally we put the results that we could formulate analytically to the test by comparing them with computer-simulations for 2D porous model systems. The structural properties, in general, are to provide useful clues for assignment and analysis of relaxation spectra. The most striking of them – the presence of negative peaks – underlines an urgent need for improvement of the current 2D Inverse Laplace Transform (ILT) algorithm used for calculation of relaxation spectra from NMR raw data.

1. Introduction

Over the past 20 years or so, multi-dimensional (MD) NMR Fourier transformation (FT) spectroscopy has grown into a versatile tool for analysis of matter [1]. All experimental techniques of the spectroscopy rely on the measurement of precession frequencies, called Larmor frequencies, of nuclear spins in an intense homogeneous and stable magnetic field to identify molecular structure and/or electronic environment of the individual atoms of chemical substances.

Over the 1D spectroscopy, which measures chemical shifts of only one of the isotopes of the substance, the MD spectroscopy has an additional advantage of establishing correlations either between Larmor frequencies and chemical shifts of different isotopes or between various chemical shifts of the same isotope in chemical compounds. This provides more detailed information on molecular structure and intra-molecular dynamics in a wide range of substances, thus making the MD FT-spectroscopy into one of the most powerful analytical methods in both chemistry [2] and structural biology [3].

Nevertheless, there are numerous systems that cannot benefit from the FT-spectroscopy either because their spectra are of no interest or because their observation is hindered by intrinsic inhomogeneity of their magnetic susceptibility. This is the case of numerous blends of, chiefly, oils and water widely used in food and cosmetics or porous media such as concretes and reservoir rocks. Furthermore there is a wealth of systems which can only be studied at what is becoming to be known as 'mobile' NMR-spectrometers, whose highly inhomogeneous magnetic field prohibits any access to FT spectroscopic data. These include NMR-equipment used in prospecting oil [4] or studying bulky samples [5,6]. In such situations, measurement of relaxation rates – phenomenological quantities describing repolarisation kinetics of macroscopic magnetisation of a system of nuclear spins along the constant field of the NMR spectrometer's magnet after an excitation by radio frequency (RF) irradiation – becomes essential. Being driven by magnetic interactions, fluctuating with time, between nuclear spins and their nearby environment [7], relaxation reveals various chemical and physical aspects of such systems.

Even in the most simple systems, several distinct relaxation times may be useful to measure: the spin-lattice relaxation time T_1, which describes how quickly the longitudinal magnetisation – the component of the magnetisation parallel to the magnetic field – returns to its equilibrium non-zero value, the spin-spin relaxation time T_2, which characterises the decrease of the transverse

* Corresponding authors. Fax: +33 (0) 1 40 43 54 50.
E-mail addresses: Dimitri.Bytchenkoff@lcpc.fr (D. Bytchenkoff), Stephane.Rodts@lcpc.fr (S. Rodts).

1090-7807/$ - see front matter © 2010 Elsevier Inc. All rights reserved.
doi:10.1016/j.jmr.2010.09.007

magnetisation – the component of the magnetisation perpendicular to the magnetic field – towards its equilibrium zero value, and the so-called time $T_{1\rho}$, which describes the relaxation of the transverse magnetisation while the system is irradiated at its resonance frequency.

These rates allowed to discriminate between various compartments, containing interstitial water, of live tissues [8] or distinguish between water and oil in emulsions [9]. They permitted to dose solid suspensions in a very large concentration range [10]. They were also used to monitor the formation of organised structures in complex systems such as cements during their setting [11,12] or ageing thixotrope fluids [13]. They proved very sensitive to phase changes and so allowed to monitor freezing and melting cycles in porous media [14]. In the field-cycling NMR, measurements of relaxation rates as a function of the field strength to which the system is exposed allowed to study, at the nanometric scale, the movements of molecules interacting with surfaces and quantify the time scales at which these movements take place [15,16]. Finally relaxation rates are used extensively to create various types of contrasts in biomedical and material science magnetic resonance imaging (MRI) [17].

Heterogeneous systems are usually characterised by distributions of relaxation times rather than one particular relaxation time. This situation could be observed when several fluids of different nature, e.g. water and oils – each having its own relaxation time – were parts of the system, or when a fluid of the same nature was confined in several rather isolated zones, or compartments, of the system with distinctly different physical properties, such as pores of different size in a porous medium or different cells in a live tissue. Nevertheless, viewed within the eigen-modes formalism (see below), the relaxation rate of even a continuous fluid in one and only cavity or in compartments connected to one another can take more than one value. This makes us think that the widely made assumption that each peak in a relaxation spectrum necessarily corresponds to a particular compartment in the system is not always justifiable.

The raw NMR-signal $M(t_i)$ of a system with a limited number N of distinct spin-spin $T_{2,n}$'s can, for instance, be expressed as a series

$$M(t_i) = \sum_{n=1}^{N} w_n \exp\left(\frac{-t_i}{T_{2,n}}\right), \quad t_i > 0 \tag{1}$$

where w_n's are the weights of the various $T_{2,n}$'s and t_i's the moments of time at which the signal was sampled by the analogue-to-digital converter (ADC). The values of $T_{2,n}$ can then be determined by fitting, in the least-square sense, the experimental data with the series of Eq. (1) [13] or by 'curve peeling' technique [18], and formed into a spectrum similar to those of chemical shift distributions in the FT-spectroscopy. The raw NMR-signal of a system with a large number of distinct $T_{2,n}$'s or with a continuous distribution $s(T)$ of $T_{2,n}$ can be formulated as a Laplace integral

$$M(t_i) = \int_T s(T) \exp\left(\frac{-t_i}{T}\right) d\ln T \tag{2}$$

Thus the calculation of the spectrum $s(T)$ consists here in differentiating the first-kind Fredholm integral in Eq. (2).

The numerical solution of this problem is notoriously unstable when applied to noise-impaired signals. To stabilise it, various inverse Laplace transformation (ILT) algorithms have been developed, viz. [19–22]. In all these algorithms, irregular solutions for $s(T)$ are dismissed as highly unlikely spectral structures and $s(T)$ is assumed to be non-negative, the latter premise being corroborated by a theoretical study [23]. In one way or another, the algorithms are aimed at finding the non-negative least-square minimum:

$$Min_{s\geqslant 0}\left\{\sum_i \left(M(t_i) - \int_T s(T)\exp\left(-\frac{t_i}{T}\right)d\ln T\right)^2 + \lambda \int_T \left(\frac{\partial^2 s}{\partial(\ln T)^2}\right)^2 d\ln T\right\} \tag{3}$$

where the Thikonov regularisation term is weighed by the parsimony coefficient λ. In general, the regularisation is applied to the square of the norm of the second derivative of the spectrum, but it could also be applied to the square of the norm of the first derivative or even to that of the spectrum itself without any notable incidence on the form of thus obtained spectrum. The coefficient λ is chosen as large as possible, making, though, sure that the covariance between the experimental data and the signal resulted from the minimisation does not exceed the experimental noise level.

These algorithms encouraged development of the 1D nuclear spin relaxation spectroscopy, or 1D ILT-spectroscopy, which has been extensively used for analysis of fruit and vegetables [24,8] as well as for studying fluids confined in porous materials. The NMR-signal of such systems stems chiefly from the interstitial fluid whose molecules can diffuse in domains delimited by solid boundaries, e.g. cell boundaries or pores surfaces, and with which they can interact in various ways, e. g. adsorption, chemical exchange, magnetic dipole-dipole coupling.

In diffusive systems (see Fig. 1) generally, the local non-equilibrium magnetisation density $m(\mathbf{r})$ of the confined fluid, to which the observable NMR-signal is proportional, can be expressed [25] by the relaxation-diffusion equation:

$$\phi(\mathbf{r})\frac{\partial m}{\partial \mathbf{t}} = \nabla \cdot \boldsymbol{D}(\mathbf{r})\nabla m - \phi(\mathbf{r})R_\alpha(\mathbf{r})m, \tag{4}$$

where ϕ, $\boldsymbol{D}$ and $R_\alpha = 1/T_\alpha$ are the local fluid concentration, diffusion tensor and relaxation rate respectively, and the subscript $\alpha = 1$, 2 or 1ρ depending on which type of relaxation it is dealt with. NMR-relaxation of the fluid driven by its interaction with the boundary between two domains A and B, and magnetisation transfer between these domains are first-order processes taken in account in the boundary condition:

$$\begin{aligned}&\boldsymbol{n}_A(\mathbf{r})\cdot\boldsymbol{D}_A(\mathbf{r})\nabla m_A - \phi_A(\mathbf{r})\rho_{A,\alpha}(\mathbf{r})m_A \\ &\quad = -\boldsymbol{n}_B(\mathbf{r})\cdot\boldsymbol{D}_B(\mathbf{r})\nabla m_B + \phi_B(\mathbf{r})\rho_{B,\alpha}(\mathbf{r})m_B = k(\mathbf{r})\cdot(m_A - m_B)\end{aligned} \tag{5}$$

where subscripts A and B denote quantities pertaining to either side of the boundary: $\boldsymbol{n}_A$ and $\boldsymbol{n}_B$ are the normal unit-vector directed towards the inside of domains A and B respectively, $\rho_{A,\alpha}$ and $\rho_{B,\alpha}$ the surface relaxation rates in either domain, also called 'relaxivities'. The latter can be significantly higher than that inside the fluid R_α. Finally $k(\mathbf{r})$ is the surface permeability. Naturally, the permeability k has to be set to zero when it deals with the boundaries between fluid and solid phases. Eqs. (4) and (5), due to the term ϕ and the

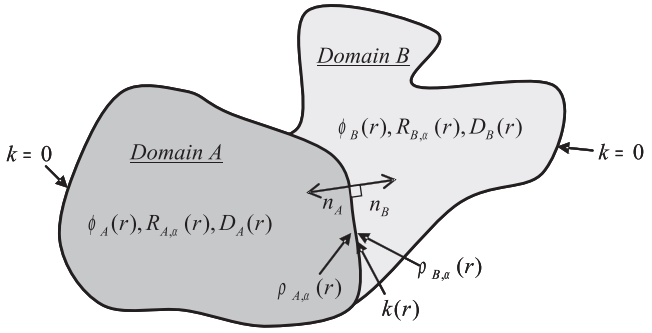

Fig. 1. Scheme of a diffusive system having two domains A and B, here delimited by solid lines, with their own individual porosity $\phi(\mathbf{r})$, relaxation rates $R_\alpha(\mathbf{r})$'s and diffusion tensor $\boldsymbol{D}(\mathbf{r})$ fields. The boundaries of the domains are characterised by surface relaxation rate $\rho_\alpha(\mathbf{r})$ and permeability $k(\mathbf{r})$.

tensorial character of $\boldsymbol{D}$, remain rather general and allow to model porous materials with nanometric confinement as well as biological tissues.

When the porous media is saturated with the fluid and has pores big enough for the diffusion of most of the fluid not to be affected by the presence of the boundaries, Eqs. (4) and (5), with all the quantities they include, can be viewed as equations that pertain to the inside of the pores only. If, moreover, one assumes that there is no exchange of fluid between pores of different size, T_α's averaged over the total volume of the pores can be found to increase with the typical diameter of the pore d and to tend asymptotically towards [25]

$$\frac{1}{T_\alpha}-\frac{1}{T_{bulk}}\propto\frac{\rho}{d}\quad\text{when}\quad\frac{\rho d}{D_{bulk}}\ll 1 \tag{6}$$

and

$$\frac{1}{T_\alpha}-\frac{1}{T_{bulk}}\propto\frac{D_{bulk}}{d^2}\quad\text{when}\quad\frac{\rho d}{D_{bulk}}\gg 1 \tag{7}$$

These two extreme cases, called 'surface limited relaxation' and 'diffusion limited relaxation' respectively, were observed in model-controlled media [26].

Due to this direct relationship between T_α's and d, the 1D ILT of relaxation data developed into a tool of choice for characterising the porous texture of cement pastes [27,18] , and water and oil in rocks [28]. On the other hand, various faults in the 1D ILT-algorithms as defined by Eq. (3) became conspicuous. In particular, the algorithms tended to break each broad component of the spectrum into several narrower components [29,12]. An attempt was made at alleviating this drawback and getting rid of the premise that there may be no negative components in the spectrum [29]. Unfortunately, the algorithm has not come into the widespread use and so inspired little further algorithm development.

The idea of the MD ILT-spectroscopy, correlating various relaxation mechanisms [30,31], emerged in the early 1980's. To acquire a T_1–T_2 spectrum (see Fig. 2), a non-equilibrium magnetisation, which most often results from an initial RF-irradiation of the sample, is allowed to relax; after a while t_1 the longitudinal magnetisation is placed in to the transverse plane by another RF-pulse and is left to relax during a while t_2; the transverse magnetisation will induce a signal:

$$M(t_1,t_2)=\iint_{T_1,T_2}s(T_1,T_2)\exp\left(-\frac{t_1}{T_1}-\frac{t_2}{T_2}\right)d\ln T_1 d\ln T_2 \tag{8}$$

This signal has been interpreted as a sum of the signals pertaining to the various domains of the inhomogeneous sample, each with its own T_1 and T_2, and so proportional to $\exp\left(-\frac{t_1}{T_2}-\frac{t_2}{T_2}\right)$. After the experiment is repeated for various, gradually incremented, $t_{1,i}$ and $t_{2,j}$, a 2D relaxation spectrum $s(T_1,T_2)$ can be obtained by the 2D ILT of the experimental data $M(t_1,t_2)$. Such spectrum allows in particular to discriminate between the sample domains sharing one of the relaxation times value. In the T_2–T_2 experiment, two periods of spin-spin relaxation are separated by a period of fixed duration, called 'mixing time', during which the spin system is subject to spin-lattice relaxation [32]. This allows for 'exchange' between the populations of spins relaxing at different T_2-rates, to which correspond different spectral lines in 1D spectra, and so for appearance of cross-peaks in 2D spectra.

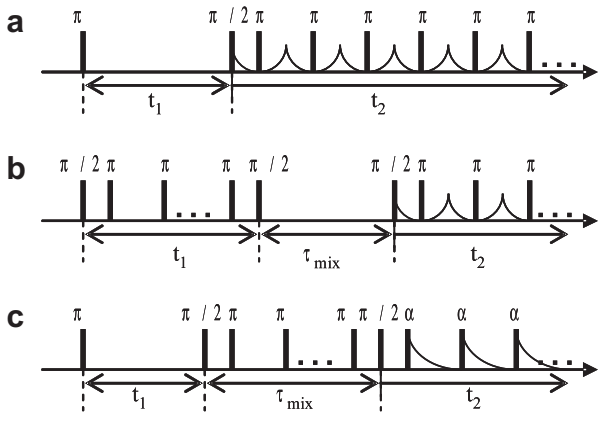

Fig. 2. NMR experimental scheme to acquire 2D (a) T_1–T_2, (b) T_2–T_2 and (c) T_1–T_1 exchange spectra.

Theoretically, both 2D FT and ILT are equivalent to corresponding two consecutive 1D transformations along time scales t_1 and t_2. In practice, though, the numerical 1D ILT-algorithms available to date make this transformation non-linear and thus cannot be used for making a 2D ILT in two steps. This made it necessary to IL-transform experimental data in one single step, which significantly slowed down the development of the 2D ILT-spectroscopy. One had to wait till 2002 for the first 2D ILT-algorithm capable of being performed on an ordinary PC [33,34]. It consists in finding the minimum:

$$Min_{s\geqslant 0}\left\{\begin{array}{l}\sum_{i,j}\left(M(t_{1,i}t_{2,j})-\iint_{T_1,T_2}s(T_1,T_2)\exp\left(-\frac{t_{1,i}}{T_1}-\frac{t_{2,j}}{T_2}\right)d\ln T_1 d\ln T_2\right)^2\\ \quad+\lambda\iint_{T_1,T_2}(s(T_1,T_2))^2 d\ln T_1 d\ln T_2\end{array}\right\} \tag{9}$$

which is a generalisation of Eq. (3). Nevertheless it still implies that the spectrum should be positive $s(T_1,T_2)$ everywhere and applies Tikhonov regularisation to the square of the norm of the spectrum.

The occurrence of the algorithm motivated numerous NMR-spectroscopists to design new pulse sequences capable of producing data necessary for various relaxation correlation T_1–T_2 [34] and exchange T_2–T_2 [35] and T_1–T_1 [36] (see Fig. 2) spectra. The ideas of these pioneering methods were further developed in designing experimental schemes for correlating different components of the diffusion tensor in porous media [37], various relaxation times and the sample's intrinsic magnetic field inhomogeneity [38], or chemical shifts [36] as well as relaxation times measured in various magnetic fields [39].

These techniques already allowed in-depth study of polymers [40], fruit and vegetables [41,36], dairy products [42], 'cement-based materials' [43], as well as water and oil in rocks [44]. Specifically, the T_1–T_2 spectra have been used to identify different domains in heterogeneous samples and to measure T_1/T_2 ratios for those domains. Knowledge of the latter proved crucial for the quantitative modelling of molecular dynamics of fluids adsorbed at surfaces [35,44]. The cross-peaks in the T_2–T_2 spectra of heterogeneous systems have most often been interpreted as an indication of exchange of matter among their various domains [35].

Two theoretical approaches have so far been taken to interpret the appearance of cross-peaks. One of them is the first-order two-site exchange model [45,35]. This phenomenological model, favoured by many physicists, allows to monitor the exchange rates by measuring the cross-peaks' intensities as a function of the mixing period [46–49]. The other is the eigen-modes formalism [50,51], in which the peaks in the spectrum are accounted for by the presence of non-zero scalar products between the spin-lattice and spin-spin eigenmodes. Being rather more abstract and implying no exchange process in principle, the latter allowed in particular to account for the presence of the diagonal and cross-peaks in such a simple system as one isolated pore, for which the former would predict the appearance of one diagonal peak only.

Nevertheless the interpretation of both 1 and 2D relaxation spectra has been seriously impeded by the faults in the

ITL-algorithms. Thus, for the reasons inherent in the algorithms, the locations of the cross-peaks in T_2–T_2 spectra were found shifted with respect to the corresponding diagonal peaks [52] and each of the broad components split into several narrower components by so-called 'pearling effect' [37]. Furthermore, unlike the 1D algorithms [53], the 2D one provides no mean to estimate the error for the spectra calculated from noise-impaired experimental data.

Thus, an improvement on the present ILT-algorithms remains the main concern for the further development of the ITL-spectroscopy [39]. In this connection, several questions have been raised over the structure of the relaxation spectra: do the spectra have to be symmetrical, anti-symmetrical or asymmetrical? Can there be peaks in the T_1–T_2 spectra for which $T_1 < T_2$? Can there be peaks with negative amplitudes in the T_1–T_2 spectra [46,50]? Can there be cross-peaks in the T_1–T_2 spectra of the systems [54] in which $T_1 = T_2$? How to maximise the cross-peaks' intensities? Answering at least some of these questions could help to design a more adequate ILT-algorithm.

Herein we shall complete our preceding work [51] and establish a number of general structural laws for the 2D relaxation spectra of diffusive systems within the eigenmodes theory. We shall also reveal some strong tendencies, rather than laws, of the spectra drawing on both the perturbation theory for sets of alike relaxation eigenmodes and the phenomenological first-order two-site exchange model. The results inferred theoretically will be put to the test by numerical simulations of the spectra of 2D model porous media. The numerical methods we used in this work will be outlined.

2. Theory: NMR-relaxation in diffusive systems

2.1. Eigenmodes formalism

2.1.1. General case

The eigenmode formalism is outlined and applied to describe nuclear spin relaxation in fluids confined in porous media. The expressions of the FID-signal generated in the T_1–T_2,T_1–T_1 and T_2–T_2 experiments as well as their spectra obtained by Laplace inversion are given.

For each of the relaxation processes α mentioned above, it is possible [55] to construct a basis of a countable number of real orthonormal eigenmodes $\psi_{\alpha,n}(\boldsymbol{r}), n = 1,2,\ldots$, i.e.

$$\int_{\boldsymbol{r}} \phi(\boldsymbol{r})\Psi_{\alpha,n}(\boldsymbol{r})\Psi_{\alpha,m}(\boldsymbol{r})d\boldsymbol{r} = \delta_{n,m}, \tag{10}$$

where the Krönecker symbol $\delta_{n,m} = 1$ when $n = m$ and $\delta_{n,m} = 0$ when $n \neq m$ – associated with eigenvalues $\tau_{\alpha,n}$ of the relaxation time t_α – so that each of them satisfies

$$-\frac{1}{\tau_{\alpha,n}}\phi(\boldsymbol{r})\Psi_{\alpha,n}(r) = \nabla\cdot\boldsymbol{D}(\boldsymbol{r})\nabla\Psi_{\alpha,n}(\boldsymbol{r}) - \phi(\boldsymbol{r})R_\alpha(\boldsymbol{r})\Psi_{\alpha,n}(\boldsymbol{r}) \quad \text{when} \quad r\in\Omega \tag{11}$$

derived from Eq. (4), and meets the condition of Eq. (5) at the boundary between two neighbouring domains A and B

$$\begin{aligned} &n_A(r)\cdot D_A(r)\nabla\Psi_{\alpha,n}(r)_A - \phi_A(r)\rho_{A,\alpha}\Psi_{\alpha,n}(r)_A \\ &\quad = -n_B(r)\cdot D_B(r)\nabla\Psi_{\alpha,n}(r)_B + \phi_B(r)\rho_{B,\alpha}(r)\Psi_{\alpha,n}(r)_B \\ &\quad = k(r)(\Psi_{\alpha,n}(r)_A - \Psi_{a,n}(r)_B) \quad \text{when} \quad r\in\partial\Omega \end{aligned} \tag{12}$$

where Ω and $\partial\Omega$ stand for the inside and the boundaries of the various domains of the system respectively.

The time-evolution of the general solution of Eq. (4) can then be formulated as

$$m(r,t) = \sum_{n=1}^{\infty} a_n\Psi_{\alpha,n}(r)\times\exp\left(-\frac{t}{\tau_{\alpha,n}}\right) \tag{13}$$

where

$$a_n = \int_{r\in\Omega}\phi(r)\Psi_{\alpha,n}(r)m(r,t=0)dr \tag{14}$$

The $\tau_{\alpha,n}$'s are unique and can be numbered so that $\tau_{\alpha,1} \geqslant \tau_{\alpha,2} \geqslant \tau_{\alpha,3} \geqslant \cdots$. Moreover, in what follows, we shall assume all $\tau_{\alpha,n}$'s to be non-degenerated, i.e. only one particular $\psi_{\alpha,n}(\boldsymbol{r})$ will be associated with each of the $\tau_{\alpha,n}$'s, as the conclusions we shall draw herein can easily be generalised for the degenerated $\tau_{\alpha,n}$'s.

As will transpire below, Eqs. (13) and (14) are more convenient to write as

$$\begin{aligned} |m(r,t)> &= \sum_n < \Psi_{\alpha,n}(r)|m(r,t=0) > \times|\Psi_{\alpha,n}(r) \\ &> \exp\left(-\frac{t}{\tau_{\alpha,n}}\right) \end{aligned} \tag{15}$$

in the 'bra-ket' notation – in which the modes $|\Psi_{\alpha,n}\rangle$ and the magnetisation state of the system $|m\rangle$ are viewed as vectors in the space of the real functions of variable $\boldsymbol{r}$ – and where we defined the scalar product as

$$\langle f|g\rangle \equiv \int_r \phi(r)f(r)g(r)dr \tag{16}$$

The signal that corresponds to the non-equilibrium part of magnetisation and which can be measured in one of the common NMR-relaxation experiments – e.g. the 'inversion-recovery' [56], to measure T_1 ; CPMG [57,58], to measure T_2 ; or experiments in the rotating frame [59,60], to measure $T_{1\rho}$–at a given moment of the time t can be written as

$$M(t) \equiv \int_r \phi(r)m(r,t)dr = \langle 1|m(t)\rangle \tag{17}$$

where $|1\rangle$ is the scalar field equal to one everywhere in the fluid phase of the system.

The initial state $|m(t=0)\rangle$ is most often proportional to $m_0|1\rangle$, where m_0 stands for the equilibrium magnetisation density. Combining Eqs. (15) and (17) [23], the non-equilibrium part of the signal can be shown to be proportional to

$$M_\alpha(t) = m_0\sum_n \langle 1|\Psi_{\alpha,n}\rangle^2\exp(-t/\tau_{\alpha_n}) \tag{18}$$

and its spectrum, after a 1D ILT, to

$$S_\alpha(T) = m_0\sum_n \langle 1|\Psi_{\alpha,n}\rangle^2\delta_{T,\tau_{\alpha,n}} \tag{19}$$

Thus the spectral lines of amplitude

$$S_{T_\alpha}(n) = m_0\langle 1|\Psi_{\alpha,n}\rangle^2 \tag{20}$$

will occur at $T = \tau_{\alpha,n}$ only and these amplitudes are positive.

Likewise, the signal in the T_1–T_2 experiment [50] can be expressed as

$$\begin{aligned} M(t_1,t_2) = m_0\sum_{n,m}&\langle 1|\Psi_{1,n}\rangle\langle\Psi_{1,n}|\Psi_{2,m}\rangle\langle\Psi_{2,m}|1\rangle \\ &\times\exp\left(-\frac{t_1}{\tau_{1,n}} - \frac{t_2}{\tau_{2,m}}\right) \end{aligned} \tag{21}$$

and the spectral lines of amplitude

$$S_{T_1-T_2}(n,m) = m_0\langle 1|\Psi_{1,n}\rangle\langle\Psi_{1,n}|\Psi_{2,m}\rangle\langle\Psi_{2,m}|1\rangle \tag{22}$$

will have the coordinates $(\tau_{1,n},\tau_{2,m})$ in the corresponding 2D spectrum.

The signal in the T_2–T_2 experiment, in which two spin-spin relaxation periods t_1 and t_2 are separated by a spin-lattice mixing period τ_{mix}, can be formulated as

$$M(t_1,t_2) = m_0 \sum_{n,m,p} \langle 1|\Psi_{2,n}\rangle\langle\Psi_{2,n}|\Psi_{1,p}\rangle\langle\Psi_{1,p}|\Psi_{2,m}\rangle\langle\Psi_{2,m}|1\rangle \times \exp\left(-\frac{t_1}{\tau_{2,n}} - \frac{\tau_{mix}}{\tau_{1,p}} - \frac{t_2}{\tau_{2,m}}\right) \quad (23)$$

and its spectral lines of amplitude

$$S_{T_2-T_2}(n,m) = m_0 \sum_{p} \langle 1|\Psi_{2,n}\rangle\langle\Psi_{2,n}|\Psi_{1,p}\rangle\langle\Psi_{1,p}|\Psi_{2,m}\rangle\langle\Psi_{2,m}|1\rangle \exp -(\tau_{mix}/\tau_{1,p}) \quad (24)$$

will have coordinates $(\tau_{2,n},\tau_{2,m})$.

Finally the signal in the T_1–T_1 experiment [36], in which a spin-spin mixing period τ_{mix} is sandwiched between two spin-lattice relaxation periods t_1 and t_2, can be written as [51]

$$M(t_1,t_2) = m_0 \sum_{n,m,p} \langle 1|\Psi_{1,n}\rangle\langle\Psi_{1,n}|\Psi_{2,p}\rangle\langle\Psi_{2,p}|\Psi_{1,m}\rangle\langle\Psi_{1,m}|1\rangle \times \exp\left(-\frac{t_1}{\tau_{1,n}} - \frac{\tau_{mix}}{\tau_{2,p}} - \frac{t_2}{\tau_{1,m}}\right) \quad (25)$$

and its spectral lines of amplitude

$$S_{T_1-T_1}(n,m) = m_0 \sum_{p} \langle 1|\Psi_{1,n}\rangle\langle\Psi_{1,n}|\Psi_{2,p}\rangle\langle\Psi_{2,p}|\Psi_{1,m}\rangle\langle\Psi_{1,m}|1\rangle \times \exp(-\tau_{mix}/\tau_{2,p}) \quad (26)$$

will have coordinates $(\tau_{1,n},\tau_{1,m})$.

It should be noted that all results reported in this section were obtained from the system of Eqs. (4) and (5) only. The latter describe nuclear spin relaxation of fluids confined in porous media or biological systems in great generality and could potentially be further generalised for some other types of systems. The eigenmode formalism can be applied to any systems described by linear equations implying exchange, diffusion and nuclear spin relaxation of the first order. This model, the main subject of the present study, can be further refined for it to be applicable to more complex systems such as blends of different types of molecule, miscible or not, confined or free and with or without magnetisation exchange, e.g. mixtures of alkanes in a test-tube (bulk hydrocarbon) or those of water and hydrocarbon in porous media. For such systems all conclusions made here will still be valid.

2.1.2. Case of similar sets of eigenmodes

The eigenmode formalism is combined with the perturbation theory to describe nuclear spin relaxation in fluids confined in porous media having alike sets of T_1- and T_2-eigenmodes.

Within the eigen-modes formalism, the vectors $|\Psi_{\alpha,n}\rangle$ can have arbitrary directions in the functional space. In practice, though, there happen to be strong correlations among the spin-lattice and spin-spin relaxation modes. In particular, $|\Psi_{1,n}\rangle$ and $|\Psi_{2,n}\rangle$ modes were shown to become similar to one another in porous media, when n's are big enough [23]. Moreover, the $R_\alpha(\boldsymbol{r})$ and $\rho_\alpha(\boldsymbol{r})$ were found experimentally to be of the same order of magnitude for various α in various systems. To take into account these particularities, we shall assume the differences between the volume fields $R_\alpha(\boldsymbol{r})$, on the one hand, and between the surface fields $\rho_\alpha(\boldsymbol{r})$, on the other hand, to be small, i.e. $R_2(\boldsymbol{r}) = R_1(\boldsymbol{r}) + \delta R(\boldsymbol{r})$, where $\delta R(\boldsymbol{r}) \ll R_1(\boldsymbol{r}) < R_2(\boldsymbol{r})$ and $\rho_2(\boldsymbol{r}) = \rho_1(\boldsymbol{r}) + \delta\rho(\boldsymbol{r})$, where $\delta\rho(\boldsymbol{r}) \ll \rho_1(\boldsymbol{r}) < \rho_2(\boldsymbol{r})$, and regard $\delta R(\boldsymbol{r})$ and $\delta\rho(\boldsymbol{r})$ as small perturbations. Applying the quantum perturbation theory [61] to the relaxation eigenmodes, we generalise here the previous results [62] and approximate $|\Psi_{2,n}\rangle$ as a linear combination of $|\Psi_{1,n}\rangle$'s:

$$|\Psi_{2,n}\rangle \approx |\Psi_{1,n}\rangle + \sum_{m\neq n} \frac{\langle\Psi_{1,m}|\delta R,\delta\rho|\Psi_{1,n}\rangle}{1/\tau_{1,n} - 1/\tau_{1,m}}|\Psi_{1,m}\rangle \quad (27)$$

where

$$\langle\Psi_{1,m}|\delta R,\delta\rho|\Psi_{1,n}\rangle = \int_{r\in\Omega} \phi(r)\delta R(r)\Psi_{1,m}(r)\Psi_{1,n}(r)dr + \int_{r\in\partial\Omega} \phi(r)\delta\rho(r)\Psi_{1,m}(r)\Psi_{1,n}(r)dS \quad (28)$$

The second-order approximation of the eigenvalues $\frac{1}{\tau_{2,n}}$ can be written as

$$\frac{1}{\tau_{2,n}} \approx \frac{1}{\tau_{1,n}} + \langle\Psi_{1,n}|\delta R,\delta\rho|\Psi_{1,n}\rangle + \sum_{m\neq n} \frac{\langle\Psi_{1,n}|\delta R,\delta\rho|\Psi_{1,m}\rangle^2}{1/\tau_{1,n} - 1/\tau_{1,m}} \quad (29)$$

and the first-order approximation of the scalar products of $|\Psi_{1,n}\rangle$ and $|\Psi_{2,n}\rangle$ as

$$\langle\Psi_{1,n}|\Psi_{2,n}\rangle \approx 1 + O(\delta R^2,\delta\rho^2) \quad (30)$$

and

$$\langle\Psi_{1,m}|\Psi_{2,n}\rangle \approx \frac{\langle\Psi_{1,m}|\delta R,\delta\rho|\Psi_{1,n}\rangle}{1/\tau_{1,n} - 1/\tau_{1,m}} \text{ when } m \neq n \quad (31)$$

2.2. First-order two-site exchange model

The Bloch–McConnell model is outlined and applied to describe nuclear spin relaxation in fluids confined in porous media. The expressions of the FID-signal generated in the T_1–T_2, T_1–T_1 and T_2–T_2 experiments as well as their spectra, obtained by Laplace inversion, are derived.

A much simpler framework to consider relaxation in diffusive media was set by analogy with the Bloch–McConnell model of the first-order chemical exchange of matter between two magnetically inequivalent sites [63,1] and has found more favour than the eigen-modes formalism with NMR-spectroscopists [45].

Within this phenomenological model, the system is supposed to have two compartments A and B of volumes V_A and V_B, each having its own relaxation time, $T_{\alpha,A}$ or $T_{\alpha,B}$ respectively. The flux of magnetisation $J_{A\to B}$ between the compartments is assumed to be engendered by and proportional to the difference between supposedly uniform magnetisation densities m_A and m_B in the compartments, i.e. $J_{A\to B} = k(m_A - m_B)$, where k is the exchange rate, independent of relaxation. A system of differential equations can then be written for m_A and m_B:

$$\begin{aligned} V_A\frac{\partial m_A}{\partial t} &= -V_A R_{\alpha,A} m_A + k(m_B - m_A) \\ V_B\frac{\partial m_B}{\partial t} &= -V_B R_{\alpha,B} m_B + k(m_A - m_B) \end{aligned} \quad (32)$$

where $R_{\alpha,A} = 1/T_{\alpha,A}$ and $R_{\alpha,B} = 1/T_{\alpha,B}$ are relaxation rates in the compartments. Note that we do not use quite the same notions as those found in literature [45,35,46–49]. The magnetisation density of the system at equilibrium is supposed to be uniform, i.e. $m_0 = m_A(t = 0) = m_B(t = 0)$, and the signal acquired in the NMR-relaxation experiments can be expressed as $M(t) = V_A m_A(t) + V_B m_B(t)$.

Previous works [46] allowed to express analytically the amplitudes of the components and their positions in the relaxation spectra as a function of the coefficients of Eq. (32). These expressions are rigorous yet rather obscure and, we believe, help little to understand the physical aspects of the system.

Here is our, phenomenologically clearer, approach to deal with the problem, where the coefficient of Eq. (32) intervene rather implicitly, though. Eq. (32) can be written more laconically as

$$\frac{\partial X}{\partial t} = \boldsymbol{K}X; \quad (33)$$

where

$$K = \begin{pmatrix} -R_{\alpha,A} - \frac{k}{V_A} & \frac{k}{\sqrt{V_A V_B}} \\ \frac{k}{\sqrt{V_A V_B}} & -R_{\alpha,B} - \frac{k}{V_B} \end{pmatrix} \text{ and } |X\rangle = \begin{pmatrix} \sqrt{V_A} m_A \\ \sqrt{V_B} m_B \end{pmatrix} \tag{34}$$

Introducing the vector

$$|1\rangle = \begin{pmatrix} \sqrt{V_A} \\ \sqrt{V_B} \end{pmatrix} \tag{35}$$

the experimental initial conditions and the measured signal can be formulated respectively as

$$|X(t=0)\rangle = m_0|1\rangle \text{ and } M(t) = \langle 1|X(t)\rangle \tag{36}$$

Thus we find ourselves in the same formal frame as that of eigenmodes, described above, except that now the system evolves in a 2D space instead of the functional space of infinite dimensionality. Being symmetric, the operator $\boldsymbol{K}$ has two orthonormal eigenmodes of general form

$$|\Psi_{\alpha,+}\rangle = \begin{pmatrix} \cos\beta_\alpha \\ \sin\beta_\alpha \end{pmatrix} \text{ and } |\Psi_{\alpha,-}\rangle = \begin{pmatrix} \sin\beta_\alpha \\ -\cos\beta_\alpha \end{pmatrix}, \tag{37}$$

which are thoroughly defined by setting the angle β_α dependent of the coefficients of the system, and whose eigenvalues we shall denote as $\tau_{\alpha,+}$ and $\tau_{\alpha,-}$ respectively. Using the identity

$$K = -\frac{1}{\tau_{\alpha,+}}|\Psi_{\alpha,+}\rangle\langle\Psi_{\alpha,+}| - \frac{1}{\tau_{\alpha,-}}|\Psi_{\alpha,-}\rangle\langle\Psi_{\alpha,-}|, \tag{38}$$

we deduce three relationships:

$$cotg(2\beta_\alpha) = \frac{\sqrt{V_A V_B}}{2}\left\{\frac{R_{\alpha,B} - R_{\alpha,A}}{k} + \frac{1}{V_B} - \frac{1}{V_A}\right\}, \tag{39}$$

$$\frac{1}{\tau_{\alpha,+}} = \frac{1}{2}\left(R_{\alpha,A} + R_{\alpha,B} + \frac{k}{V_A} + \frac{k}{V_B}\right) - \frac{k}{\sqrt{V_A V_B}\sin 2\beta_\alpha} \text{ and} \tag{40}$$

$$\frac{1}{\tau_{\alpha,-}} = \frac{1}{2}\left(R_{\alpha,A} + R_{\alpha,B} + \frac{k}{V_A} + \frac{k}{V_B}\right) + \frac{k}{\sqrt{V_A V_B}\sin 2\beta_\alpha}; \tag{41}$$

It appears to be possible to chose the value of β_α within $0 \leqslant \beta_\alpha < \pi/2$. Either eigenvalue can be shown to be positive, though.

Eq. (39) indicates that β_α is a decreasing function of $dR_\alpha = R_{\alpha,B} - R_{\alpha,A}$ (see Fig. 3), while Eqs. (40) and (41) show that $|\Psi_{\alpha,+}\rangle$ is always the fundamental state of the system with

$$\tau_{\alpha,+} \geqslant \tau_{\alpha,-} \geqslant 0 \tag{42}$$

The state $|1\rangle$ can be rewritten as

$$|1\rangle = \sqrt{V_A + V_B}\begin{pmatrix} \cos\beta_0 \\ \sin\beta_0 \end{pmatrix} \tag{43}$$

where the angle β_0 satisfies $0 \leqslant \beta_0 < \pi/2$ and

$$cotg(2\beta_0) = \frac{\sqrt{V_A V_B}}{2}\left\{\frac{1}{V_B} - \frac{1}{V_A}\right\} \tag{44}$$

The introduction of β_0 and β_α allows to express concisely the scalar products between $|\psi_{\alpha,+}\rangle, |\psi_{\alpha,-}\rangle$ and $|1\rangle$ (see Fig. 4):

$$\begin{aligned} \langle 1|\Psi_{\alpha,+}\rangle &= \sqrt{V_A + V_B}\cos(\beta_\alpha - \beta_0) \\ \langle 1|\psi_{\alpha,-}\rangle &= \sqrt{V_A + V_B}\sin(\beta_\alpha - \beta_0) \end{aligned} \tag{45}$$

Comparing Eqs. (39) and (44), we notice that $\beta_\alpha = \beta_0$ when $dR_\alpha = 0$. This remarkable property will allow us to analyse the signs of the scalar products as a function of the sign of dR_α, and, ultimately, those of the difference between the relaxation times $T_{\alpha,A}$ and $T_{\alpha,B}$.

The relaxation spectra can be calculated by drawing on the results of the eigen-modes formalism. Two spectral lines of amplitudes

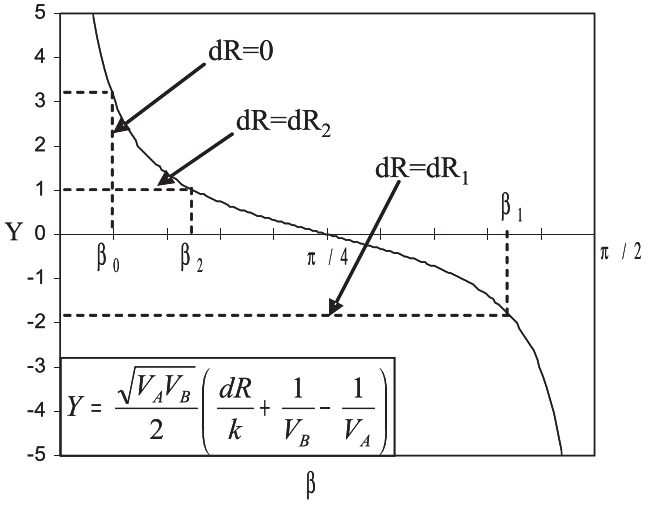

Fig. 3. Dimensionless, second term Y in Eq. (39) as a function of β_α. The magnitudes of the quantities dR_1, dR_2, β_0, β_1 and β_2 were chosen arbitrarily.

$$\begin{aligned} S_\alpha(\tau_{\alpha,+}) &= m_0(V_A + V_B)\cos^2(\beta_\alpha - \beta_0) \\ S_\alpha(\tau_{\alpha,-}) &= m_0(V_A + V_B)\sin^2(\beta_\alpha - \beta_0) \end{aligned} \tag{46}$$

will appear at the coordinates $\tau_{\alpha,+}$ and $\tau_{\alpha,-}$ in the 1D T_α-spectrum.

The four components of the T_1–T_2 spectrum will be:

$$\begin{aligned} S_{T_1-T_2}(\tau_{1,+},\tau_{2,+}) &= m_0(V_A + V_B)\cos(\beta_1 - \beta_0)\cos(\beta_2 - \beta_1)\cos(\beta_2 - \beta_0) \\ S_{T_1-T_2}(\tau_{1,+},\tau_{2,-}) &= m_0(V_A + V_B)\cos(\beta_1 - \beta_0)\sin(\beta_2 - \beta_1)\sin(\beta_2 - \beta_0) \\ S_{T_1-T_2}(\tau_{1,-},\tau_{2,+}) &= -m_0(V_A + V_B)\sin(\beta_1 - \beta_0)\sin(\beta_2 - \beta_1)\cos(\beta_2 - \beta_0) \\ S_{T_1-T_2}(\tau_{1,-},\tau_{2,-}) &= m_0(V_A + V_B)\sin(\beta_1 - \beta_0)\cos(\beta_2 - \beta_1)\sin(\beta_2 - \beta_0) \end{aligned} \tag{47}$$

where β_1 and β_2 are the angles β_α calculated for spin-lattice and spin-spin relaxation, respectively. Finally the components of the T_2–T_2 spectrum are:

$$S_{T_2-T_2}(\tau_{2,+},\tau_{2,+}) = m_0(V_A + V_B)\cos^2(\beta_2 - \beta_0)\left\{\cos^2(\beta_2 - \beta_1)\exp\left(-\frac{\tau_{mix}}{\tau_{1,+}}\right) + \sin^2(\beta_2 - \beta_1)\exp\left(-\frac{\tau_{mix}}{\tau_{1,-}}\right)\right\}$$

$$\begin{aligned} S_{T_2-T_2}(\tau_{2,+},\tau_{2,-}) &= S_{T_2-T_2}(\tau_{2,-},\tau_{2,+}) \\ &= m_0(V_A + V_B)\cos(\beta_2 - \beta_0)\sin(\beta_2 - \beta_0) \\ &\quad \cos(\beta_2 - \beta_1)\sin(\beta_2 - \beta_1)\left\{\exp\left(-\frac{\tau_{mix}}{\tau_{1,+}}\right) - \exp\left(-\frac{\tau_{mix}}{\tau_{1,-}}\right)\right\} \end{aligned}$$

$$S_{T_2-T_2}(\tau_{2,-},\tau_{2,-}) = m_0(V_A + V_B)\sin^2(\beta_2 - \beta_0)\left\{\sin^2(\beta_2 - \beta_1)\exp\left(-\frac{\tau_{mix}}{\tau_{1,-}}\right) + \cos^2(\beta_2 - \beta_1)\exp\left(-\frac{\tau_{mix}}{\tau_{1,-}}\right)\right\} \tag{48}$$

and those of the T_1–T_1 spectrum:

$$S_{T_1-T_1}(\tau_{1,+},\tau_{1,+}) = m_0(V_A + V_B)\cos^2(\beta_1 - \beta_0)\left\{\cos^2(\beta_2 - \beta_1)\exp - \left(\frac{\tau_{mix}}{\tau_{2,+}}\right) + \sin^2(\beta_2 - \beta_1)\exp\left(-\frac{\tau_{mix}}{\tau_{2,-}}\right)\right\}$$

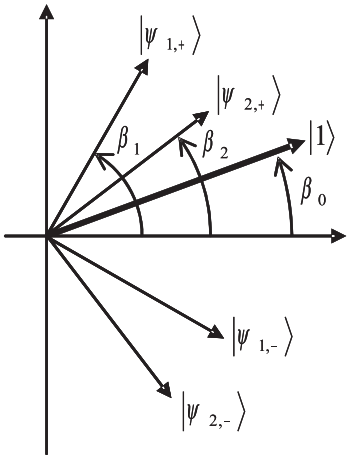

Fig. 4. 2D vector representation of the eigen-modes, $|\Psi_{1,+}\rangle$,$|\Psi_{1,-}\rangle$,$|\Psi_{2,+}\rangle$ and $|\Psi_{2,-}\rangle$ as well as the uniform state as a function of the angles β_0,β_1 and β_2.

$$S_{T_1-T_1}(\tau_{1,+},\tau_{1,-}) = S_{T_1-T_1}(\tau_{1,-},\tau_{1,+}) = -m_0(V_A+V_B)\cos(\beta_1-\beta_0)\sin(\beta_1-\beta_0)\cos(\beta_2-\beta_1)\sin(\beta_2-\beta_1)\left\{\exp\left(-\frac{\tau_{mix}}{\tau_{2,+}}\right)-\exp\left(-\frac{\tau_{mix}}{\tau_{2,-}}\right)\right\}$$

$$S_{T_1-T_1}(\tau_{1,-},\tau_{1,-}) = m_0(V_A+V_B)\sin^2(\beta_1-\beta_0)\left\{\sin^2(\beta_2-\beta_1)\exp\left(-\frac{\tau_{mix}}{\tau_{2,+}}\right)+\cos^2(\beta_2-\beta_1)\exp\left(-\frac{\tau_{mix}}{\tau_{2,-}}\right)\right\} \quad (49)$$

3. Numerical methods

The finite-difference time-domain numerical approach is outlined and applied to find approximate solution of the diffusion-relaxation equation system. The algorithm we used to find eigenmodes and eigenvalues as well as our method of simulation of relaxation spectra are described.

The finite-difference time-domain (FDTD) approach [64] can be applied to find numerically solutions of Eqs. (4) and (5) and to deduce eigenmodes. Thus found modes can be introduced into Eqs. (20), (22), (24) and (26) to simulate the relaxation spectra.

3.1. Solving the diffusion–relaxation equations

If we assume that all relaxation processes and diffusion that take place in the system are uniform and isotropic, i.e. that R_α's and ρ_α's are independent of $\boldsymbol{r}$ and $\boldsymbol{D}$ is a scalar constant, and limit ourselves to the 2D porous systems, Eqs. (4) and (5) will become simply

$$\frac{\partial m}{\partial t} = D\Delta m - R_\alpha m \quad (50)$$

and

$$\boldsymbol{n}D\nabla m = \rho m \quad (51)$$

The FDTD allows to find approximate solutions of these equations and consists in the partition of the 2D system into square pixels of the side length δx by a Cartesian mesh (see Fig. 5). Two types of pixel are so generated: 'empty' pixels, corresponding to the pores, and 'filled' pixels, corresponding to the solid matrix. Starting from an initial state of magnetisation $m_{i,j}(t=0)$ in the centres of the pixels of coordinates (i,j), magnetisation $m_{i,j}(t_n)$ is calculated iteratively at discrete moments $t_n = n\delta t$, $n = 1,2,3\ldots$. For an 'empty' pixel (i,j) whose neighbouring pixels on the left, on the right, above and below are also 'empty' (Fig. 6a), the iterative formula is

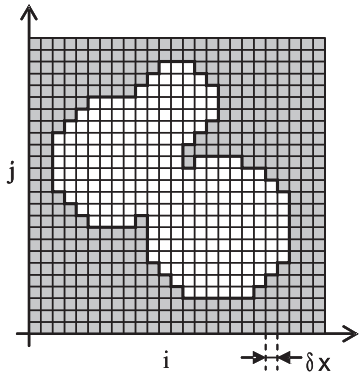

Fig. 5. 2D porous system divided into square cases by a Cartesian mesh. White and grey pixels represent the pores' inside and the solid matrix respectively.

$$m_{i,j}(t_{n+1}) = m_{i,j}(t_n) + D\delta t\left\{\frac{m_{i+1,j}(t_n)+m_{i-1,j}(t_n)+m_{i,j+1}(t_n)+m_{i,j-1}(t_n)-4m_{i,j}(t_n)}{\delta x^2}\right\} \quad (52)$$

When one of the neighbouring pixel of the pixel (i,j), e.g. $(i-1,j)$ is 'filled' (Fig. 6b), $m_{i-1,j}(t_n)$ in Eq. (52) is substituted – as it was previously done in 1D simulations [65] – by a fictitious magnetisation state

$$\tilde{m}_{i-1,j}(t_n) = \frac{2\rho - D\delta x}{2\rho + D\delta x} m_{i,j}(t_n) \quad (53)$$

so that the discretised boundary condition

$$D\frac{m_{i,j}(t_n)+\tilde{m}_{i-1,j}(t_n)}{2} = \rho\frac{m_{i,j}(t_n)-\tilde{m}_{i-1,j}(t_n)}{\delta x} \quad (54)$$

is met at the interface $(i-1/2,j)$ between these two pixels.

If the pixel (i,j) is in a corner (Fig. 6c), e.g. when both $(i-1,j)$ and $(i,j-1)$ are 'filled', then not only $m_{i-1,j}(t_n)$, but also $m_{i,j-1}(t_n)$ have to be replaced by the fictitious states $\tilde{m}_{i-1,j}(t_n)$ and $\tilde{m}_{i,j-1}(t_n)$ in Eq. (52). Mention should be made, though, that such corners are most often a pure product of the present numerical method, in which smooth boundaries of the system are fragmented into parts parallel to either the axis $\vec{i}$ or the axis $\vec{j}$ the orthogonal Cartesian

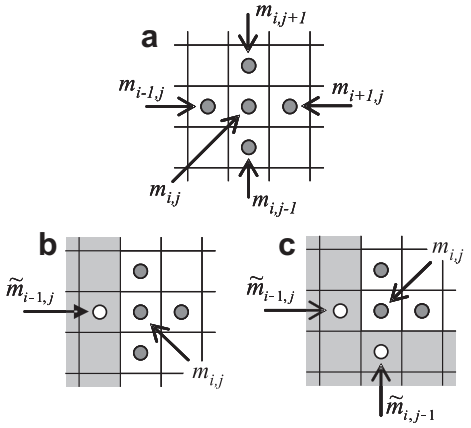

Fig. 6. Three types of neighbourhood to the pore's boundary in which the pixel can be found: pixel (i,j) is (a) surrounded by 'empty' pixels only, (b) next to a 'filled' pixel and (c) next to two 'filled' pixels. White and grey pixels represent the pores' inside and the solid matrix respectively. Round grey and white spots in the centre of pixels indicate, respectively, the locations where magnetisation is calculated and set to a fictitious value to fulfil the boundary conditions.

frame. Using the expression of Eq. (53) for the fictitious magnetisations would result in overestimating the effect of the boundary on relaxation of the nearby interstitial fluid wherever the genuine boundary was not parallel to one of the axes of the Cartesian frame. To alleviate this problem, the surface relaxation rate ρ in Eq. (53) should be weighed by the factor $\frac{1}{\sqrt{2}}$:

$$\tilde{m}_{i-1,j}(t_n) = \tilde{m}_{i,j-1}(t_n) = \frac{\rho\sqrt{2} - D\delta x}{\rho\sqrt{2} + D\delta x} m_{i,j}(t_n) \tag{55}$$

With thus defined $\tilde{m}_{i-1,j}(t_n)$ and $\tilde{m}_{i,j-1}(t_n)$, the impact of the boundary on the relaxation will be taken into account adequately when it is parallel to either of the axes or to the bisector of the angle between them. For the boundaries tilted otherwise with respect to the axes, the error will also be significantly smaller than that which would be generated by the use of Eq. (53). The situations where the pixel has three or four 'filled' neighbouring pixels (not shown here) are dealt with similarly.

The time increment was set according to

$$\delta t = \frac{1}{8}\frac{\delta x^2}{D} \tag{56}$$

to ensure stability and reasonable precision of the programme and to avoid generation of spurious modes.

3.2. Finding eigenmodes

The relaxation eigenmodes can be numerically approximated in a way similar to that in which vibration eigenmodes of fractal drums were previously determined [66].

An arbitrary initial magnetisation state $m_{i,j}(t_0 = 0)$ is injected into the discrete diffusion-relaxation equation, Eq. (52), to calculate the state at the moment $t_1 = \delta t$ in time. This new state $m_{i,j}(t_1)$ is injected into Eq. (52) to calculate the state at the moment $t_2 = 2\delta t$. Carrying on this iterative process will reveal the time-evolution of the system's magnetisation, analytically expressed by Eq. (15). After a while long enough, all the members of the sum in Eq. (15) superior to the first will have faded away owing to the exponentially decreasing factors and Eq. (15) will become

$$|m_{i,j}(t \to \infty)\rangle \approx \langle \Psi_{\alpha,1}|m_{i,j}(t=0)\rangle |\Psi_{\alpha,1}\rangle \exp\left(-\frac{t}{\tau_{\alpha,1}}\right), \tag{57}$$

from where the fundamental mode $|\Psi_{\alpha,1}\rangle$ can be obtained by renormalising $|m_{i,j}(t \to \infty)\rangle$. The eigen-time $\tau_{\alpha,1}$ is determined by comparing the amplitudes of the states $|m(t)\rangle$ and $|m(t+\delta t)\rangle$. Other modes and times are sought for in a similar manner. To find the next, say (N+1)th mode, the initial state $m_{i,j}(t_1 = 0)$ is first projected on to the subspace orthogonal to the N modes already found:

$$\begin{aligned} |m'(t=0)\rangle &= |m(t=0)\rangle - \sum_{n=1}^{N} \langle \Psi_n | m(t=0)\rangle \times |\Psi_n\rangle \\ &= \sum_{n=N+1}^{\infty} \langle \Psi_n | m(t=0)\rangle \times |\Psi_n\rangle \end{aligned} \tag{58}$$

and this projection is then injected into Eq. (52).

3.3. Simulation of relaxation spectra

To simulate 2D relaxation spectra, two series of eigenmodes $|\Psi_{1,n}\rangle$ and $|\Psi_{2,n}\rangle$, $1 \leqslant n \leqslant N$, are calculated as described in the previous section for two surface relaxation rates ρ_1 and ρ_2, depending on whether it deals with spin-lattice or spin-spin relaxation. Only a limited number N of modes can effectively be calculated. This limitation, as can be seen from Eq. (22), will result in restricting observation of the T_1–T_2 spectra to the zone where $T_1, T_2 \geqslant \tau_{1,N}, \tau_{2,N}$ only. On the other hand, it will introduce an error:

$$\begin{aligned} &\left| S_{T_2-T_2}(n,m) - m_0 \sum_{p=1}^{N} \langle 1|\Psi_{2,n}\rangle\langle\Psi_{2,n}|\Psi_{1,p}\rangle\langle\Psi_{1,p}|\Psi_{2,m}\rangle\langle\Psi_{2,m}|1\rangle \exp(-\tau_{mix}/\tau_{1,p}) \right| \\ &= \left| m_0 \sum_{p=N+1}^{\infty} \langle 1|\Psi_{2,n}\rangle\langle\Psi_{2,n}|\Psi_{1,p}\rangle\langle\Psi_{1,p}|\Psi_{2,m}\rangle\langle\Psi_{2,m}|1\rangle \exp(-\tau_{mix}/\tau_{1,p}) \right| \\ &\leqslant m_0 |\langle 1|\Psi_{2,n}\rangle\langle\Psi_{2,m}|1\rangle| \sqrt{1 - \sum_{p=1}^{N} |\langle\Psi_{1,p}|\Psi_{2,n}\rangle|^2} \\ &\quad \times \sqrt{1 - \sum_{p=1}^{N} |\langle\Psi_{1,p}|\Psi_{2,m}\rangle|^2} \exp\left(-\frac{\tau_{mix}}{\tau_{1,N}}\right) \end{aligned} \tag{59}$$

in the T_2–T_2 spectra as the infinite sum in Eq. (24) is approximated by the finite sum:

$$\begin{aligned} S_{T_2-T_2}(n,m) \approx m_0 \sum_{p=1}^{N} &\langle 1|\Psi_{2,n}\rangle\langle\Psi_{2,n}|\Psi_{1,p}\rangle\langle\Psi_{1,p}|\Psi_{2,m}\rangle\langle\Psi_{2,m}|1\rangle \\ &\times \exp(-\tau_{mix}/\tau_{1,p}) \end{aligned} \tag{60}$$

In practice, though, these errors have turned out to be smaller than round-off error of our computer. A similar error occurs in the T_1–T_1 spectra.

4. Results and discussion

4.1. General properties of the relaxation spectra

We developed further [51] the use of eigen-modes formalism for description of 2D relaxation spectra, pioneered by Song et al. [50]. The expressions we deduced within the formalism make conspicuous a number of structural properties shared by all relaxation spectra independently of the system to study. Few of these properties were already reported [51], though often with no proper analytical prove. Hereafter, we give an extended list of, this time, thoroughly proved properties of the spectra.

(a) Cross-peaks in the 2D spectra

When $|\Psi_{1,n}\rangle$'s and $|\Psi_{2,n}\rangle$'s are identical – which does not necessarily mean that $\tau_{1,n}$'s and $\tau_{2,n}$'s are so as well – the scalar products $\langle\Psi_{2,n}|\Psi_{1,m}\rangle$'s are equal to zero for $n \neq m$ and the T_1–T_2 spectra will contain diagonal peaks, of intensity

$$S_{T_1-T_2}(n,n) = m_0 \langle 1|\Psi_{2,n}\rangle^2, \tag{61}$$

only, as

$$S_{T_1-T_2}(n,m) = 0 \text{ when } n \neq m \tag{62}$$

The same goes for the T_2–T_2 and T_1–T_1 spectra:

$$S_{T_2-T_2}(n,m) = m_0 \delta_{n,m} \langle 1|\Psi_{2,n}\rangle^2 \exp(-\tau_{mix}/\tau_{1,n}) \tag{63}$$

$$S_{T_1-T_1}(n,m) = m_0 \delta_{n,m} \langle 1|\Psi_{1,n}\rangle^2 \exp(-\tau_{mix}/\tau_{2,n}) \tag{64}$$

Thus spin-lattice and spin-spin relaxation processes must be different enough for cross-peaks to occur in the spectra.

Furthermore the observation of cross-peaks in T_1–T_1 and T_2–T_2 spectra requires 'mixing': if $\tau_{mix} = 0$ then

$$S_{T_2-T_2}(n,m) = m_0 \langle 1|\Psi_{2,n}\rangle\langle\Psi_{2,m}|1\rangle \sum_p \langle\Psi_{2,n}|\Psi_{1,p}\rangle\langle\Psi_{1,p}|\Psi_{2,m}\rangle \tag{65}$$

or – owing to the closure relationship

$$\sum_p |\Psi_{1,p}\rangle\langle\Psi_{1,p}| = Id \tag{66}$$

for the orthonormal bases – more simply

$$S_{T_2-T_2}(n,m) = m_0\langle 1|\Psi_{2,n}\rangle\langle\Psi_{2,n}|\Psi_{2,m}\rangle\langle\Psi_{2,m}|1\rangle = m_0\delta_{n,m}\langle 1|\Psi_{2,n}\rangle^2, \quad (67)$$

which indicates that only diagonal peaks will appear in the spectrum. The same goes for the T_1–T_1 spectra. Thus, even when $|\Psi_{1,n}\rangle$ and $|\Psi_{2,n}\rangle$ are different, there may be no cross-peaks in the spectrum, unless τ_{mix} is properly chosen.

(*b*) *Symmetry of the 2D spectra*

The T_1–T_1 and T_2–T_2 spectra are always symmetrical:

$$S_{T_1-T_1}(n,m) = S_{T_1-T_1}(m,n) \quad (68)$$

and

$$S_{T_2-T_2}(n,m) = S_{T_2-T_2}(m,n) \quad (69)$$

which can be deduced from Eqs. (24) and (26).

This important property was not verified in the pioneering work [35] in the subject, where the T_2–T_2 spectra obtained using the algorithm available at the time [33] were asymmetric. Now such asymmetry can surely be accounted for faults in experimental protocols or data processing, rather than for any particular properties of the studied system.

(*c*) *Overall intensity of the 2D spectra*

The overall intensity of the T_1–T_2 spectrum corresponds to the total magnetisation of the sample at equilibrium:

$$\sum_{n,m} S_{T_1-T_2}(n,m) = m_0\langle 1|1\rangle \quad (70)$$

where $\langle 1|1\rangle = \int\phi(r)dr$ is the total volume occupied by fluid in the sample and where we used Eq. (66) in summing the intensities of all components in the spectrum.

Similarly, the overall intensity of the T_2–T_2 spectrum corresponds to the magnetisation which would remain, should the system be subject to longitudinal relaxation during the period τ_{mix} only, as in the inversion-recovery experiment:

$$\sum_{n,m} S_{T_2-T_2}(n,m) = m_0\sum_n\langle 1|\Psi_{1,n}\rangle^2\exp(-\tau_{mix}/\tau_{1,n}) = M_1(\tau_{mix}) \quad (71)$$

Finally, the overall intensity of the T_1–T_1 spectrum corresponds to the magnetisation which would remain, should the system be subject to transverse relaxation during the period τ_{mix} only, as in the CPMG experiment:

$$\sum_{n,m} S_{T_1-T_1}(n,m) = M_2(\tau_{mix}) \quad (72)$$

This property makes clear the difference between information that can be extracted from the intensities of the T_1–T_2 and T_2–T_2 spectra. This difference was already observed experimentally: the intensities of the T_1–T_2 spectra of cements during their setting were found remarkably invariable, while those of the T_2–T_2 spectra were evolving markedly [46].

(*d*) *Conditions for eigenmodes to reveal themselves in the spectra*

Both 1 and 2D spectra provide information on the same relaxation eigenmodes $|\Psi_{1,n}\rangle$'s and $|\Psi_{2,n}\rangle$'s and so it is quite natural to expect that the spectra are related to each other in one way or another.

First, as was pointed out previously, there can be peaks only in those locations of the spectra where their coordinates correspond to the eigenvalues $\tau_{1,n}$'s and $\tau_{2,n}$'s.

Second, as the scalar product $\langle 1|\Psi_{2,n}\rangle$ intervenes as a multiplicative factor in the expression for the intensity of peaks in both the 1D T_2 and 2D T_1–T_2 spectra, a particular $|\Psi_{2,n'}\rangle$ will not manifest itself as a peak in either spectrum unless $\langle 1|\Psi_{2,n'}\rangle \neq 0$. This also holds when read another way round, i.e. if $\langle 1|\Psi_{2,n'}\rangle \neq 0$, then $|\Psi_{2,n'}\rangle$ will give rise to a peak in both the 1D and 2D spectra. This is obviously true for the 1D T_2-spectrum, as here the intensity of the peak corresponding to $|\Psi_{2,n'}\rangle$ can be written as $m_0\langle 1|\Psi_{2,n'}\rangle^2$. For the 2D T_1–T_2 spectra, one can consider its projection on to T_2 axis:

$$\sum_n S_{T_1-T_2}(n,n') = m_0\langle 1|\Psi_{2,n'}\rangle^2 = S_{T_2}(n') \quad (73)$$

and notice that, if $\langle 1|\Psi_{2,n'}\rangle \neq 0$, then at least one term in the sum on the left hand side of this equation is not equal to zero as well. For the T_2–T_2 spectra, we can express the intensity of the diagonal peaks as

$$S_{T_2-T_2}(n',n') = m_0\langle 1|\Psi_{2,n'}\rangle^2\sum_p \langle\Psi_{2,n'}|\Psi_{1,p}\rangle^2\exp\left(-\frac{\tau_{mix}}{\tau_{1,p}}\right) \quad (74)$$

whose right hand side is a sum of positive terms only. Thus it would suffice to show that one of these terms is not zero to prove that so is the intensity of the diagonal peak. This is indeed the case: since $\langle\Psi_{2,n'}|\Psi_{2,n'}\rangle = 1$ and $|\Psi_{1,n}\rangle$'s constitute an orthonormal basis, the Parseval relationship $\langle\Psi_{2,n'}|\Psi_{2,n'}\rangle^2 = \sum_p\langle\Psi_{2,n'}|\Psi_{1,p}\rangle^2 = 1$ can be written, which implies that at least one of $\langle\Psi_{2,n'}|\Psi_{1,p}\rangle$'s is not zero and thus our statement is proved. The same holds for spin-lattice eigenmodes in the 1D T_1-spectrum and the 2D T_1–T_2 and T_1–T_1 spectra.

(*e*) *Relationships between the 1 and 2D spectra*

Moreover, as can bee seen from Eq. (73), projecting the T_1–T_2 spectrum on to T_1- or T_2-axis will result in a 1D T_1- or T_2-spectrum, respectively:

$$\sum_m S_{T_1-T_2}(n,m) = m_0\langle 1|\Psi_{1,n}\rangle^2 = S_{T_1}(n)$$

$$\sum_n S_{T_1-T_2}(n,m) = S_{T_2}(m) \quad (75)$$

Similar relationships can be established between the T_1–T_1 and T_2–T_2 spectra and their projections on to the coordinate axes:

$$\sum_m S_{T_1-T_1}(n,m) = m_0\sum_p\langle 1|\Psi_{1,n}\rangle\langle\Psi_{1,n}|\Psi_{2,p}\rangle\langle\Psi_{2,p}|1\rangle \times\exp\left(-\frac{\tau_{mix}}{\tau_{2,p}}\right) = \sum_p S_{T_1-T_2}(n,p)\exp\left(-\frac{\tau_{mix}}{\tau_{2,p}}\right) \quad (76)$$

and

$$\sum_n S_{T_2-T_2}(n,m) = m_0\sum_p\langle 1|\Psi_{2,n}\rangle\langle\Psi_{2,n}|\Psi_{1,p}\rangle\langle\Psi_{1,p}|1\rangle \times\exp\left(-\frac{\tau_{mix}}{\tau_{1,p}}\right) = \sum_p S_{T_1-T_2}(p,n)\exp\left(-\frac{\tau_{mix}}{\tau_{1,p}}\right) \quad (77)$$

Finally, if we assume that none of $|\Psi_{1,n}\rangle$'s is orthogonal to $|1\rangle$, i.e., $\langle 1|\Psi_{1,n}\rangle \neq 0$ a relationship between the corresponding terms in the T_1–T_2 and T_2–T_2 spectra can be establish:

$$S_{T_2-T_2}(n,m) = m_0 \sum_p \frac{\langle 1|\Psi_{2,n}\rangle\langle\Psi_{2,n}|\Psi_{1,p}\rangle\langle\Psi_{1,p}|1\rangle\langle 1|\Psi_{1,p}\rangle\langle\Psi_{1,p}|\Psi_{2,m}\rangle\langle\Psi_{2,m}|1\rangle}{\langle\Psi_{1,p}|1\rangle^2} \times \exp\left(-\frac{\tau_{mix}}{\tau_{1,p}}\right) = \sum_p \frac{S_{T_1-T_2}(p,n)S_{T_1-T_2}(p,m)}{S_{T_1}(p)} \exp\left(-\frac{\tau_{mix}}{\tau_{1,p}}\right)$$

A similar relation can be written for the T_1–T_1 spectra.

Thus, all relaxation spectra are interdependent: Eq. (75) shows that the 1D spin-lattice and spin-spin spectra can be calculated from the T_1–T_2 spectrum; to lesser extent, Eq. (78) – which holds only when all spin-lattice modes are visible, i.e. $\langle 1|\Psi_{1,n}\rangle \neq 0$ – indicates that both T_1–T_1 and T_2–T_2 spectra can, independently of the τ_{mix} length, be calculated from the T_1–T_2 spectrum and so the latter contains maximum of information about the system that can possibly be obtain by relaxation measurements.

(f) *Signs of the spectral components in 1 and 2D spectra*

According to Eq. (20), the intensities of the spectral lines in the 1D spectra can be either positive or zero. This feature is peculiar to the 1D spectra, though. Eqs. (22), (24) and (26) do not preclude the appearance of peaks with negative intensities in the 2D spectra. While the 2D ILT algorithm available to date does exactly the opposite, T_1–T_2 spectra with negative peaks have been simulated for a system consisting of one slit-like pore [50].

In this section, we shall clarify the situation for the T_1–T_2 spectra within the eigen-modes formalism and making no assumption about the form of the diffusive system: we shall prove that such spectra, should they contain cross components, will always contain peaks with negative intensities. The case of the T_1–T_1 and T_2–T_2 spectra will be dealt with further below making use of the perturbation theory and within the first-order two-site exchange model. Here we shall limit ourselves to pointing out that Eq. (74) implies that all the diagonal peaks have non-negative intensities.

It is first and foremost for their cross-peaks that T_1–T_2 spectra are acquired. For such peaks to occur, the $|\Psi_{1,n}\rangle$ and $|\Psi_{2,n}\rangle$ sets must be different. Furthermore, unless the system is symmetric, $\langle 1|\Psi_{1,n}\rangle \neq 0$ and $\langle 1|\Psi_{2,n}\rangle \neq 0$ for any n and it is always possible to make them strictly positive by changing the sign of some of the modes. Then, at least, some of the terms $u_{n,m} = \langle\Psi_{1,n}|\Psi_{2,m}\rangle$ of the unitary matrix $U = (u_{n,m})$ will not be equal to zero, and as $|\Psi_{2,n}\rangle$ are orthogonal to each other, the coefficients $u_{n,m}$ will verify

$$\sum_p u_{n,p}u_{m,p} = 0 \tag{79}$$

for given n and m. Quite clearly, Eq. (79) cannot be satisfied unless at least one $u_{n',m'}$ of the coefficients is negative and so we can write

$$S_{T_1-T_2}(n',m') = m_0\langle 1|\Psi_{1,n'}\rangle u_{n',m'}\langle\Psi_{2,m'}|1\rangle < 0 \tag{80}$$

This proves that at least one of the components of the T_1–T_2 spectrum will have negative intensity. A mathematically more rigorous proof of the statement, though possible, is beyond the scope of the present manuscript.

(g) *Relative intensities of the diagonal and cross-peaks in the T_1–T_1 and T_2–T_2 spectra*

It has become a habit to single out groups of four peaks, called 'exchange squares', of which two, indexed (n,n) and (m,m), are diagonal and two other, indexed (n,m) and (m,n), cross-peaks. As was shown in *a* of the present section, the squares are always symmetric with respect to the diagonal. In the T_2–T_2 spectra of heterogeneous samples, cross-peaks $(n\ ,\ m)$ and $(m\ ,\ n)$ have most often been interpreted as the presence of exchange of matter between two domains n and m, whatever they are, and which we shall, hereafter, associate with modes $|\Psi_{2,n}\rangle$ and $|\Psi_{2,m}\rangle$. The measurement of the intensities of these peaks as a function of the τ_{mix} length was proposed as a method for studying kinetics of the exchange [47]. The method encouraged search for experimental conditions that would boost intensity of the cross-peaks [49]. The latter was never reported to exceed 30% of the overall intensity of the 'exchange square', though [46]. In this section, we shall prove that, in any 'exchange square', the sum of the absolute values of the intensities of the cross-peaks cannot exceed that of the diagonal peaks.

Indeed, we obtain

$$|\langle 1|\Psi_{2,n}\rangle\langle\Psi_{2,n}|\Psi_{1,p}\rangle\langle\Psi_{1,p}|\Psi_{2,m}\rangle\langle\Psi_{2,m}|1\rangle| \leqslant \frac{\langle 1|\Psi_{2,n}\rangle^2\langle\Psi_{2,n}|\Psi_{1,p}\rangle^2 + \langle\Psi_{1,p}|\Psi_{2,m}\rangle^2\langle\Psi_{2,m}|1\rangle^2}{2} \tag{81}$$

by setting $a = \langle 1|\Psi_{2,n}\rangle\langle\ \Psi_{2,n}|\Psi_{1,p}\rangle$ and $b = \langle\ \Psi_{1,p}|\Psi_{2,m}\rangle\langle\Psi_{2,m}|1\rangle$ in the well-known inequality $|ab| \leqslant (a^2 + b^2)/2$. Multiplying Eq. (80) by $\exp(-\tau_{mix}/\tau_{1,p})$ and summing over p gives

$$\sum_p |\langle 1|\Psi_{2,n}\rangle\langle\Psi_{2,n}|\Psi_{1,p}\rangle\langle\Psi_{1,p}|\Psi_{2,m}\rangle\langle\Psi_{2,m}|1\rangle| \exp\left(-\frac{\tau_{mix}}{\tau_{1,p}}\right) \leqslant \frac{S_{T_2-T_2}(n,n) + S_{T_2-T_2}(m,m)}{2m_0}, \tag{82}$$

The latter combined with Eq. (24) gives

$$|S_{T_2-T_2}(n,m)| = |S_{T_2-T_2}(m,n)| < \frac{1}{2}(S_{T_2-T_2}(n,n) + S_{T_2-T_2}(m,m)), \tag{83}$$

which corresponds to our statement.

By studying the subject within the first-order two-site exchange model (see below), we shall show that the 50% limit established here for the total relative intensity of the cross-peaks can indeed be achieved experimentally.

Note also that, when there is a cross-peak (n,m) in a spectrum, then there exists an index p' for which $\langle 1|\Psi_{2,n}\rangle\langle\Psi_{2,n}|\Psi_{1,p'}\rangle\ \langle\Psi_{1,p'}|\Psi_{2,m}\rangle\langle\Psi_{2,m}|1\rangle \neq 0$ in Eq. (24). From this we deduce that $\langle 1|\Psi_{2,n}\rangle\langle\Psi_{2,n}|\Psi_{1,p'}\rangle \neq 0$ and $\langle 1|\Psi_{2,n}\rangle\langle\Psi_{2,n}|\Psi_{1,p'}\rangle \neq 0$, and from Eq. (74) that $s_{T_2-T_2}(n,n) \neq 0$ and $s_{T_2-T_2}(m,m) \neq 0$. Thus, whatever the intensities of the cross-peaks are, there are always diagonal peaks corresponding them, of which at least one is, due to Eq. (83), more intense than any of the cross-peaks.

Finally, when the 50% limit is reached, i.e. when

$$|S_{T_2-T_2}(n,m)| = |S_{T_2-T_2}(m,n)| = \frac{1}{2}(S_{T_2-T_2}(n,n) + S_{T_2-T_2}(m,m)), \tag{84}$$

and taking into account that

$$|s_{T_2-T_2}(n,m)| \leqslant m_0 \sum_p |\langle 1|\Psi_{2,n}\rangle\langle\Psi_{2,n}|\Psi_{1,p}\rangle\langle\Psi_{1,p}|\Psi_{2,m}\rangle\langle\Psi_{2,m}|1\rangle \exp\left(-\frac{\tau_{mix}}{\tau_{1,p}}\right), \tag{85}$$

then necessarily:

$$|s_{T_2-T_2}(n,m)| = m_0 \sum_p |\langle 1|\Psi_{2,n}\rangle\langle\Psi_{2,n}|\Psi_{1,p}\rangle\langle\Psi_{1,p}|\Psi_{2,m}\rangle\langle\Psi_{2,m}|1\rangle \exp\left(-\frac{\tau_{mix}}{\tau_{1,p}}\right), \tag{86}$$

and

$$m_0 \sum_p |\langle 1|\Psi_{2,n}\rangle\langle\Psi_{2,n}|\Psi_{1,p}\rangle\langle\Psi_{1,p}|\Psi_{2,m}\rangle\langle\Psi_{2,m}|1\rangle \exp\left(-\frac{\tau_{mix}}{\tau_{1,p}}\right) = \frac{1}{2}(s_{T_2-T_2}(n,n) + s_{T_2-T_2}(m,m)), \quad (87)$$

The latter, taking into account Eq. (81), is met only when

$$|\langle 1|\Psi_{2,n}\rangle\langle\Psi_{2,n}|\Psi_{1,p}\rangle\langle\Psi_{1,p}|\Psi_{2,m}\rangle\langle\Psi_{2,m}|1\rangle| = \frac{\langle 1|\Psi_{2,n}\rangle^2\langle\Psi_{2,n}|\Psi_{1,p}\rangle^2 + \langle\Psi_{1,p}|\Psi_{2,m}\rangle^2\langle\Psi_{2,m}|1\rangle^2}{2} \quad (88)$$

for any p. And Eq. (88) itself holds only when

$$|\langle 1|\Psi_{2,n}\rangle\langle\Psi_{2,n}|\Psi_{1,p}\rangle| = |\langle\Psi_{1,p}|\Psi_{2,m}\rangle\langle\Psi_{2,m}|1\rangle| \quad (89)$$

for any p. From this we deduce that the four peaks of the 'exchange square' have equal intensities:

$$\begin{aligned} |s_{T_2-T_2}(n,m)| &= |s_{T_2-T_2}(m,n)| \\ &= \sum_p |\langle 1|\Psi_{2,n}\rangle\langle\Psi_{2,n}|\Psi_{1,p}\rangle|^2 \exp\left(-\frac{\tau_{mix}}{\tau_{1,p}}\right) \\ &= \sum_p |\langle\Psi_{1,p}|\Psi_{2,m}\rangle\langle\Psi_{2,m}|1\rangle|^2 \exp\left(-\frac{\tau_{mix}}{\tau_{1,p}}\right) \\ &= s_{T_2-T_2}(n,n) = s_{T_2-T_2}(m,m) \end{aligned} \quad (90)$$

In simulated and experimentally acquired spectra reported so far [46,49], the intensities of the cross-peaks were well below their theoretical maximum. Moreover, one of the diagonal peaks was invariably much more intense than the other. Our work shows that, when intensities of the cross-peaks approach their theoretical maximum, those of the diagonal peaks become similar to one another. The same holds for the T_1–T_1 spectra.

4.2. 2D relaxation spectra in case of alike sets of eigenmodes

In porous media, phenomenologically different spin-lattice and spin-spin relaxations are both reliant on the same diffusive process and so their respective sets of eigenmodes often turn out rather similar to each other. In such situation, one can take advantage of the formulae provided by the perturbation theory, given in Section 2.1.2, to establish a number of approximative expressions – complementary to those determined exclusively within the eigen-modes formalism – for the forms that 2D spectra can take (Fig. 7).

The zero-order approximation to the intensity of the diagonal peaks of the T_1–T_2 spectra is

$$s_{T_1-T_2}(n,n) \approx m_0\langle\Psi_{1,n}|1\rangle^2 \quad (91)$$

Similarly, the first-order approximation to the intensity of the cross-peaks of the spectra is

$$s_{T_1-T_2}(n,m\neq n) \approx m_0\langle\Psi_{1,n}|1\rangle\langle\Psi_{1,m}|1\rangle\frac{\langle\Psi_{1,m}|\delta R,\delta\rho|\Psi_{1,n}\rangle}{1/\tau_{1,n}-1/\tau_{1,m}} \quad (92)$$

The diagonal components – being the only to have the zero-order term – will be more intense than their cross counterparts. This, indeed, was observed in cements [35].

A striking feature of the spectra that can be deduced from Eq. (92) is their anti-symmetry with respect to the diagonal:

$$s_{T_1-T_2}(n,m) \approx -s_{T_1-T_2}(m,n) \quad \text{for } m\neq n \quad (93)$$

This shows that there are as many negative as there are positive cross-peaks and corroborates our prediction, made in (1c) of the present section, of ineluctable presence of peaks with negative intensities in the T_1–T_2 spectra. In practice, the ineptitude of the 2D ILT-algorithm at producing peaks of negative intensity could account for the fact that (positive) cross-peaks were so far observed only in that half of the coordinate plane where $T_1 > T_2$. The anti-symmetry given by Eq. (93) is silent as to whether it was accidental or not that all peaks with intensities of the same sign bunched together on one side of the diagonal. It suggests, however, that equally intense negative peaks should have appeared on the opposite side of the diagonal from the positive components visible in the spectra [35].

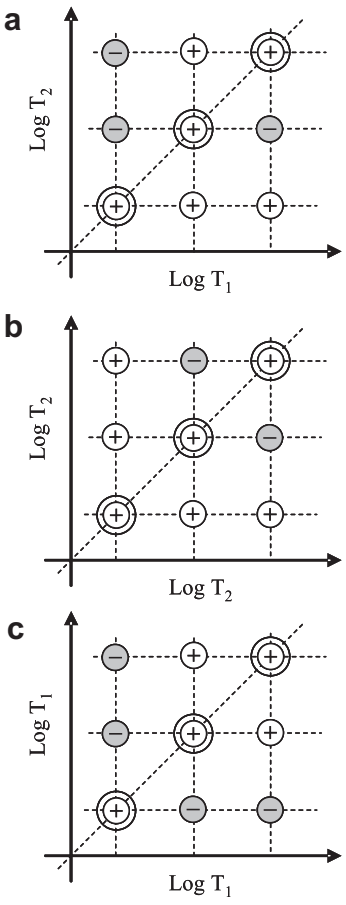

Fig. 7. 2D (a) correlation T_1–T_2, and exchange (b) T_2–T_2 and (c) T_1–T_1 relaxation spectra as predicted by the perturbation theory. The diagonal peaks are intense (bigger rounds) and positive (white rounds) in all three spectra. The T_1–T_2 spectrum is anti-symmetric, while the T_2–T_2 and T_1–T_1 are symmetric. The positive and negative peaks are coloured in white and grey respectively.

The first-order approximations to the intensity of the cross and diagonal components of the T_1–T_1 and T_2–T_2 spectra are, respectively,

$$s_{T_2-T_2}(n,m\neq n) \approx m_0\langle\Psi_{1,n}|1\rangle\langle\Psi_{1,m}|1\rangle\frac{\langle\Psi_{1,n}|\delta R,\delta\rho|\Psi_{1,m}\rangle}{1/\tau_{1,n}-1/\tau_{1,m}}\left\{\exp\left(-\frac{\tau_{mix}}{\tau_{1,n}}\right)-\exp\left(-\frac{\tau_{mix}}{\tau_{1,m}}\right)\right\} \quad (94)$$

$$s_{T_2-T_2}(n,n) \approx m_0\langle\Psi_{1,n}|1\rangle^2\exp\left(-\frac{\tau_{mix}}{\tau_{1,n}}\right) \quad (95)$$

and

$$s_{T_1-T_1}(n,m\neq n) \approx -m_0\langle\Psi_{1,n}|1\rangle\langle\Psi_{1,m}|1\rangle\frac{\langle\Psi_{1,n}|\delta R,\delta\rho|\Psi_{1,m}\rangle}{1/\tau_{1,n}-1/\tau_{1,m}}\left\{\exp\left(-\frac{\tau_{mix}}{\tau_{2,n}}\right)-\exp\left(-\frac{\tau_{mix}}{\tau_{2,m}}\right)\right\} \quad (96)$$

$$s_{T_2-T_2}(n,n) \approx m_0\langle\Psi_{1,n}|1\rangle^2\exp\left(-\frac{\tau_{mix}}{\tau_{2,n}}\right), \quad (97)$$

from where we obtain

$$s_{T_2-T_2}(n,m\neq n)\approx s_{T_1-T_2}(n,m)\left\{\exp\left(-\frac{\tau_{mix}}{\tau_{1,n}}\right)-\exp\left(-\frac{\tau_{mix}}{\tau_{1,m}}\right)\right\} \tag{98}$$

$$s_{T_1-T_1}(n,m\neq n)\approx -s_{T_1-T_2}(n,m)\left\{\exp\left(-\frac{\tau_{mix}}{\tau_{2,n}}\right)-\exp\left(-\frac{\tau_{mix}}{\tau_{2,m}}\right)\right\} \tag{99}$$

and

$$s_{T_2-T_2}(n,n)\approx s_{T_1-T_2}(n,n)\exp\left(-\frac{\tau_{mix}}{\tau_{1,n}}\right) \tag{100}$$

$$s_{T_1-T_1}(n,n)\approx s_{T_1-T_2}(n,n)\exp\left(-\frac{\tau_{mix}}{\tau_{2,n}}\right) \tag{101}$$

Not only these expressions verify the symmetry elements established above, but also corroborate the relationships between the T_1–T_2 spectrum and the T_1–T_1 and T_2–T_2 spectra. Within the perturbation theory, each of them can be calculated from either of the two other and so each of them contain exactly the same information about the system. In the present case, the cross-peaks in each of the spectra are all proportional to their counterparts in the other spectra.

The T_1–T_2 spectrum – despite its being often regarded as a correlation and not an exchange spectrum – contains as much information on the exchange phenomena that take place in the system as do the T_1–T_1 and T_2–T_2 spectra. Moreover, from Eqs. (97) and (98), one can see that the cross-peaks in the T_1–T_2 spectrum are the most intense and so the T_1–T_2 spectrum has the best signal-to-noise ratio. Thus, to the extent to which the result – obtained here within the perturbation theory – can be generalised, the very use of the exchange T_1–T_1 and T_2–T_2 spectra to study exchange becomes questionable.

Finally, we uncover an additional symmetry between signs of the cross-peaks in the exchange spectra. For $n < m$ and so, to the zero-order, for $\tau_{1,n}=\tau_{2,n}>\tau_{1,m}=\tau_{2,m}$, the $s_{T_2-T_2}(n,m)$ component has the same sign as the $s_{T_1-T_2}(n,m)$ component, while the $s_{T_1-T_1}(n,m)$ component has the opposite sign. Thus the cross-peaks in the T_1–T_1 and T_2–T_2 spectra have opposite signs. This is again consistent with the reported experimental data [35], where to the cross-peak in the T_1–T_2 spectrum, situated in the zone where $T_1 > T_2$, corresponded a pair of positive cross-peaks in the T_2–T_2 spectrum.

4.3. 2D spectra of systems with matter exchange between pairs of domains

Quantitative analysis of cross-peaks in the experimentally acquired exchange spectra has so far been carried out within the first-order two-site exchange model [46–49]. In this phenomenological model, the spectrum is regarded as a set of separate 'exchange squares', each of which being assigned to two particular domains of the system between which exchange of matter is supposed to take place. In other terms, it can be viewed as a particular kind of relaxation eigenmodes model in which each of the modes is supposed to correspond to one particular domain of the system and to be able to couple with only one other of the modes.

The structural properties of the 2D spectra as determined by Eqs. (47)–(49) within the two-site exchange model are in perfect accord with those established within the eigen-modes formalism, e.g. the exchange spectra are symmetric and their diagonal components have positive intensities. However, any attempt to apply the two-site exchange model to a network of three and more domains exchanging matter – or, in other words, to three or more coupled modes – would fail [D'Espinose, personal communication].

Likewise, the two-site exchange model also allows to rediscover the features of the spectra found within the perturbation theory. Indeed, by setting $\beta_1 \approx \beta_2$, which implies that the spin-lattice and spin-spin eigenmodes sets are similar to one another, the T_1–T_2 and T_2–T_2 spectra can be approximated to the first-order with respect to $\delta\beta = \beta_2 - \beta_1$ as

$$\begin{aligned}
&s_{T_1-T_2}(\tau_{1,+},\tau_{2,+})\approx m_0(V_A+V_B)\cos^2(\beta_1-\beta_0)\\
&s_{T_1-T_2}(\tau_{1,+},\tau_{2,-})\approx -s_{T_1-T_2}(\tau_{1,-},\tau_{2,+})\approx m_0(V_A+V_B)\cos(\beta_1-\beta_0)\\
&\qquad\qquad \sin(\beta_1-\beta_0)\delta\beta\\
&s_{T_1-T_2}(\tau_{1,-},\tau_{2,-})=m_0(V_A+V_B)\sin^2(\beta_1-\beta_0)
\end{aligned} \tag{102}$$

and

$$\begin{aligned}
&S_{T_2-T_2}(\tau_{2,+},\tau_{2,+})\approx m_0(V_A+V_B)\cos^2(\beta_1-\beta_0)\exp\left(-\frac{\tau_{mix}}{\tau_{1,+}}\right)\\
&{}^{S}T_2-T_2(\tau_{2,+},\tau_{2,-})\approx m_0(V_A+V_B)\cos(\beta_1-\beta_0)\sin(\beta_1-\beta_0)\\
&\qquad\qquad \delta\beta\left\{\exp\left(-\frac{\tau_{mix}}{\tau_{1,+}}\right)-\exp\left(-\frac{\tau_{mix}}{\tau_{1,-}}\right)\right\}\\
&{}^{S}T_2-T_2(\tau_{2,-},\tau_{2,-})\approx m_0(V_A+V_B)\sin^2(\beta_1-\beta_0)\exp\left(-\frac{\tau_{mix}}{\tau_{1,-}}\right)
\end{aligned} \tag{103}$$

Thus we find again that the T_1–T_2 spectrum is anti-symmetric with respect to the diagonal and that the components of the T_1–T_2 spectrum are proportional to their counterparts in the T_2–T_2 spectrum.

In general, Eqs. (47)–(49) allow to easily find out the sign of the components of the spectra. Note that $\{\exp(-\tau_{mix}/\tau_{1,+})-\exp(-\tau_{mix}/\tau_{1,-})\}$ and $\{\exp(-\tau_{mix}/\tau_{2,+})-\exp(-\tau_{mix}\ \tau_{2,-})\}$are positive as$\tau_{1,+}\geqslant\tau_{1,-}$ and $\tau_{2,+}\geqslant\tau_{2,-}$. Moreover all cosines that intervene in the expressions are positive as the angles β_0, β_1 and β_2 were defined to vary within $[0,\pi/2]$, while the sign of the sines will depend on the relative values of the angles. From Fig. 3, the sign of the components of the spectra can be seen to depend on the relative values of the quantities 0, $dR_1 = 1/R_{1,B} - 1/R_{1,A}$ and $dR_2 = 1/R_{2,B} - 1/R_{2,A}$ only.

Remarkablly, the laws found within the perturbation approach for the signs of the components hold here when dR_1 and dR_2 have the same sign (Fig. 8a and c). In porous media – where relaxation in the interstitial fluid is mainly due to relaxation at the interface between the fluid and the solid matrix – T_1 and T_2 can reasonably be assumed to be proportional to one onother with the quotient that typically ranges between one and ten. Then $dR_2/dR_1 > 1$ and we can expect that spectra will most often assume the form of Fig. 8c. This was indeed observed experimentally in cements, where the T_1–T_2 spectrum contained a prositive cross-peak within the zone where $T_1 > T_2$ and the T_2–T_2 spectrum contained a pair of positive cross-peaks [35]. When dR_1 and dR_2 have oposite signs, i.e. when $T_{1,B} > T_{1,A}$ and $T_{2,B} < T_{2,A}$ or $T_{1,B} < T_{1,A}$ and $T_{2,B} > T_{2,A}$ – the situation that cannot be dealt with within the perturbation theory – a negative peak appears on the diagonal of the T_1–T_2 spectrum (Fig. 8b). Such situation could possibly occur in systems with wide ranges of T_1/T_2 varying from one domain to another, like in sedimentary rocks containing clay clusters or complex biological systems.

Finally, the factor $\exp(-\tau_{mix}/\tau_{1,-})$ in Eqs. (48) and (49) reduces the intensities of the diagonal peaks, while increasing those of the cross-peaks. Thus, acquiring spectra with τ_{mix} much longer than $\tau_{1,-}$ will result in relatively stronger diagonal peaks:

$$\begin{aligned}
I_{relT_2-T_2}&=\frac{{}^{S}T_2-T_2(\tau_{2,+},\tau_{2,-})}{{}^{S}T_2-T_2(\tau_{2,+},\tau_{2,+})+{}^{S}T_2-T_2(\tau_{2,-},\tau_{2,-})}\\
&=\frac{\sin(2(\beta_2-\beta_0))\sin(2(\beta_2-\beta_1))}{2+2\cos(2(\beta_2-\beta_0))\cos(2(\beta_2-\beta_1))}
\end{aligned} \tag{104}$$

Likewise, the relative intensity of the peaks in the T_1–T_1 spectrum at long τ_{mix} :

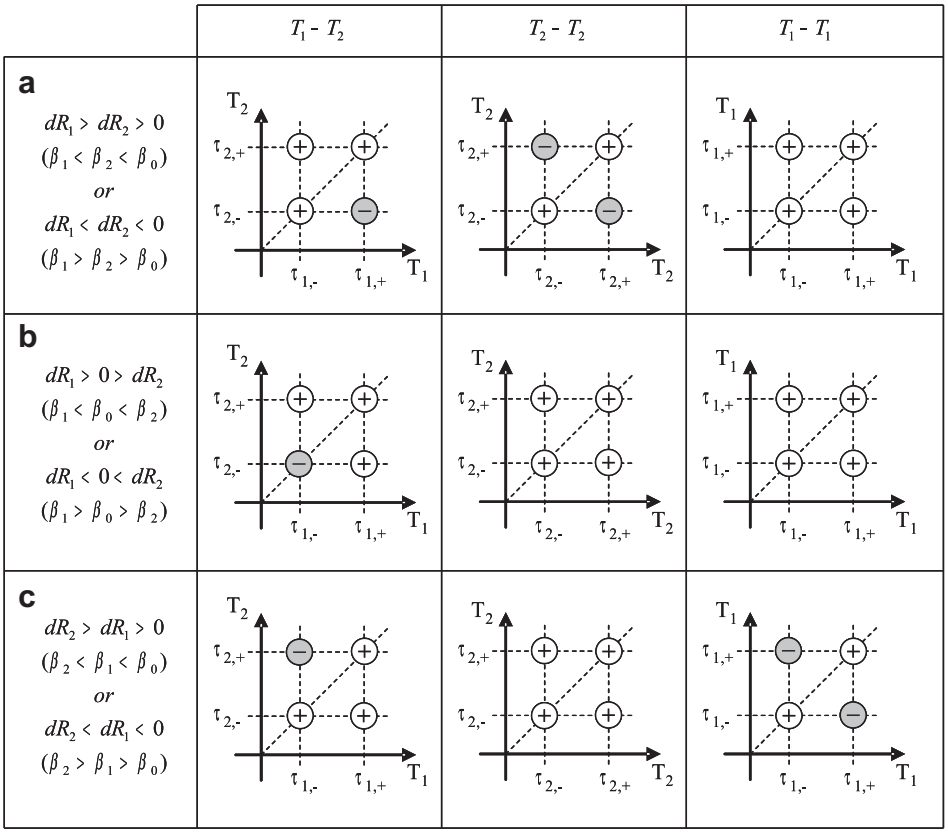

Fig. 8. Signs of the various components in the exchange spectra as a function of $dR_1 = 1/T_{1,B} - 1/T_{1,A}$ and $dR_2 = 1/T_{2,B} - 1/T_{2,A}$ as predicted by the two-site exchange model. The signs are independent of τ_{mix}.

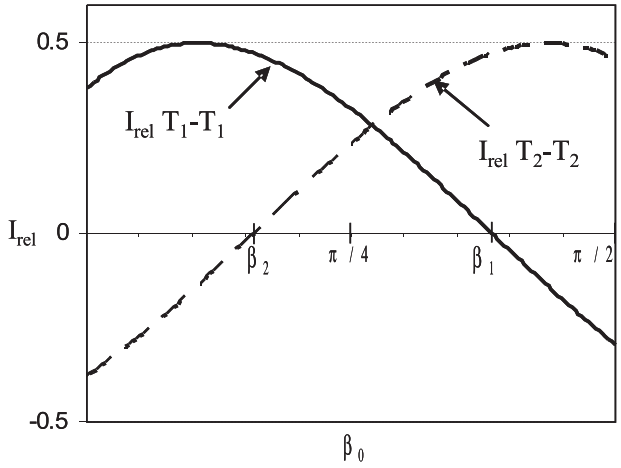

Fig. 9. Evolution the relative intensity of the cross-peaks in the T_1–T_1 (continuous line) and T_2–T_2 (dashed line) spectra as a function of β_0 in the limit of long τ_{mix} and for two arbitrary values of β_1 and β_2 . The limit of +50% is reached for a particular value of β_0 , while that of −50% could not quite be achieved.

$$I_{relT_1-T_1} = \frac{{}^{S}T_1 - T_1(\tau_{1,+},\tau_{1,-})}{{}^{S}T_1 - T_1(\tau_{1,+},\tau_{1,+}) + {}^{S}T_1 - T_1(\tau_{1,-},\tau_{1,-})} = -\frac{\sin(2(\beta_1-\beta_0))\sin(2(\beta_2-\beta_1))}{2+2\cos(2(\beta_1-\beta_0))\cos(2(\beta_2-\beta_1))} \quad (105)$$

These relative intensities can be shown to vary between + and −50% (Fig. 9). The former limit can be achieved when $2\beta_2 = \beta_0 + \beta_1 + \pi(n + 1/2)$ and $2\beta_1 = \beta_0 + \beta_2 + \pi(n + 1/2)$, where n is integer, for the T_2–T_2 and T_1–T_1 spectra, respectively. The latter limit can, in theory, be reached when $\beta_0 = \beta_1 + \pi(n + 1/2)$ and $\beta_0 = \beta_2 + \pi(n + 1/2)$ for the T_2–T_2 and T_1–T_1 spectra, respectively. In practice, though, it turns out impossible as β_0 is restrained to $[0, \pi/2]$.

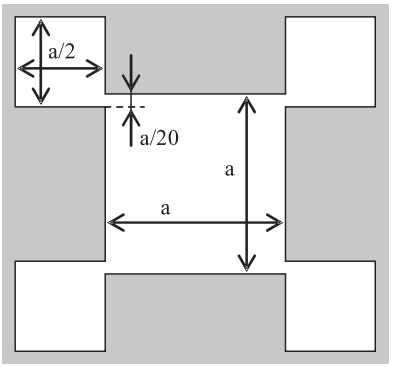

Fig. 10. Model porous media used in the simulations with pores coloured in white and solid matrix in grey. In our simulations, $a = 5$ μm.

5. Numerical simulations

The algorithm of the numerical method described in Section 3 was coded in Fortran 95 programming language. To test our programme, we used it to solve Eq. (4) and calculate up to a 100 eigenmodes satisfying the boundary condition of Eq. (5) for several geometrically simple 1 and 2D model porous systems for which the boundary problem can be solved analytically. Our programme passed this preliminary test: it turned out quick and the relative

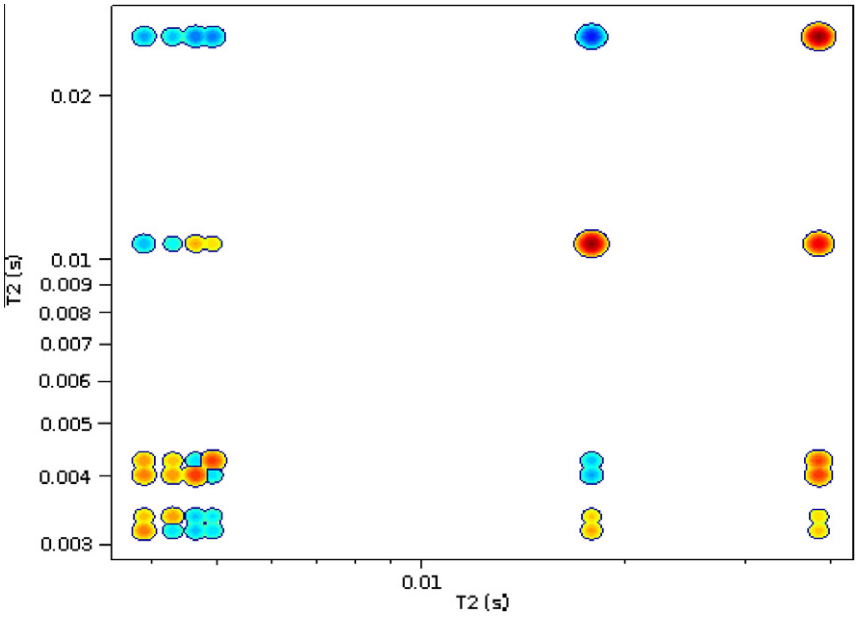

Fig. 11. The T_1–T_2 spectrum of the model porous system of Fig. 10 simulated as explained in Section 3.

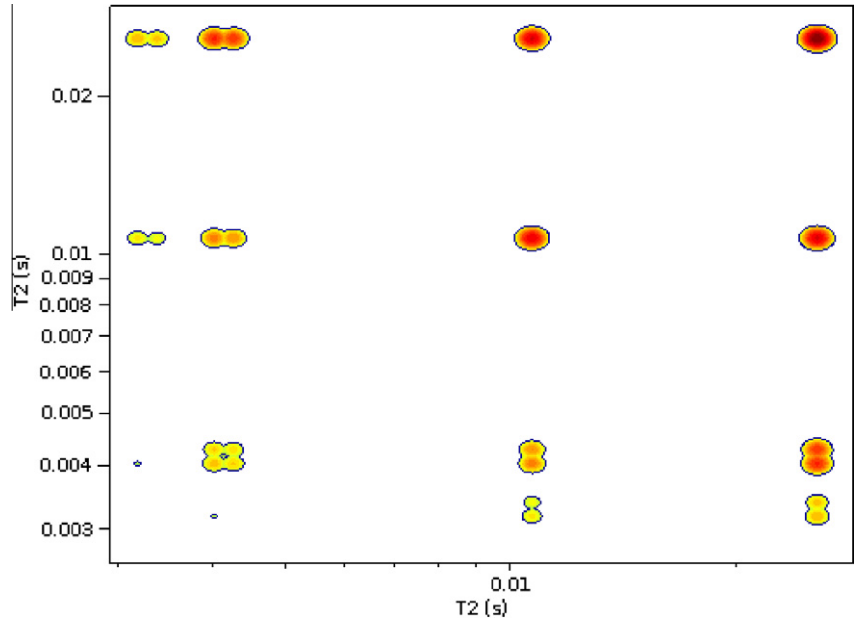

Fig. 12. The T_2–T_2 spectrum of the model porous system of Fig. 10 simulated as explained in Section 3.

error in the eigenvalues did not exceed 1% and that in the eigenmodes was even smaller.

To put the general laws we discovered theoretically to the proof, we simulated 2D relaxation spectra of the model porous system of Fig. 10 as described in Section 3. Herein we shall content ourselves with a brief discussion of T_1–T_2 and T_2–T_2 spectra. A thorough numerical analysis of all three types of 2D relaxation spectrum will be the subject of a separate manuscript (in preparation).

The square system of side length of ten micrometer was divided into ten thousand square pixels of side length δx equal to hundred nanometer by a Cartesian mesh. The diffusion coefficient D and surface longitudinal ρ_1 and transverse ρ_2 relaxation rates were set to $10^{-10}\,m^2/s$, $4\times10^{-5}\,m/s$ and $8\times10^{-5}\,m/s$, respectively. The inherent relaxation time – measure of kinetics of relaxation driven by interactions that take place inside the interstitial fluid and unrelated to its interactions with the solid matrix – was set to 0.1 s. The T_2–T_2 spectrum was calculated by setting $\tau_{mix} = 0.1$ s.

Thus calculated T_1–T_2 and T_2–T_2 spectra – shown in Figs. 11 and 12, respectively – have a large number of diagonal and cross-peaks – whose intensities are presented in Tables 1 and 2. They reflect interactions among various eigenmodes for each of the relaxation processes, rather than exchange among different compartment of the system as the number of diagonal peaks in the spectra exceed that of the compartments. All the features of the correlation and exchange spectra predicted within the perturbation approach reveal themselves in the T_1–T_2 spectrum of Fig. 11: the diagonal peaks have positive intensities; except for the pairs of peaks (3,4) and (4,3), and (5,6) and (6,5) – the positive and negative cross-peaks form a anti-symmetric pattern. The cross-peaks located symmetrically with respect to the diagonal in the T_1–T_2

Table 1
Calculated intensities of the peaks of the T_1–T_2 spectrum of Fig. 11. The indices n and m here number the peaks of Fig. 11 from the right to the left and from the top to the bottom respectively. The values for the least intense peaks should only be regarded as an indication of their order of magnitude because of the approximations introduced by the FDTD-method.

6	5	4	3	2	1	n/m
−0.000490	−0.000200	−0.002300	−0.001400	−0.029000	0.440000	1
−0.000280	−0.000041	0.000140	0.000038	0.370000	0.034000	2
0.000280	0.000090	−0.000100	0.003600	−0.000170	0.002900	3
0.000650	0.000310	0.005500	−0.000079	−0.000360	0.004900	4
0.000078	0.000240	−0.000160	−0.000054	0.000053	0.000042	5
0.000630	0.000088	−0.000200	−0.000098	0.000160	0.000070	6

Table 2
Calculated intensities of the peaks of the T_2–T_2 spectrum of Fig. 12. The indices n and m here number the peaks of Fig. 12 from the right to the left and from the top to the bottom respectively. The values for the least intense peaks should only be regarded as an indication of their order of magnitude because of the approximations introduced by the FDTD-method.

6	5	4	3	2	1	n/m
0.0001100	0.0000650	0.0075000	0.0044000	0.0490000	0.6800000	1
0.0000220	0.0000096	0.0005400	0.0003200	0.0360000	0.0490000	2
		0.0000490	0.0000290	0.0003200	0.0044000	3
0.0000012		0.0000820	0.0000490	0.0005400	0.0075000	4
				0.0000096	0.0000650	5
		0.0000012		0.0000220	0.0001100	6

spectrum (see Table 1) have intensities of the same order of magnitude. Furthermore, viewed within the first-order two-site exchange model, the simulated spectra exemplify the situation of Fig. 8c: most positive cross-peaks in the T_1–T_2 spectrum of Fig. 11 are in the zone where the T_1 is longer than T_2; in the the T_2–T_2 spectrum of Fig. 12, most peaks are positive. Nevertheless the spectra contain some features that have not been reported before: the correlation spectrum T_1–T_2 contains some negatives peaks, though of low intensity, in the domain where $T_1 > T_2$; there are also weak negative components in the exchange T_2–T_2 spectrum. This must be a direct consequence of including a mixing period during which the system evolves under longitudinal relaxation, and that the sign of the scalar products that intervene in the formulae describing the structure of the T_2–T_2 spectra are not under full control of the spectroscopist running the experiment and can be made either positive or negative. For the time being we cannot give a more physical explanation of this phenomenon.

6. Conclusion

We studied the exchange spectra within the eigen-modes formalism and our investigation revealed a number of general laws that determine the structure of the spectra. Here are the most striking of them:

(a) the exchange spectra are symmetric;
(b) there can be no cross-peak with no diagonal peaks that correspond to it;
(c) the 1D and 2D spectra are interdependent;
(d) where the perturbation theory is applicable, the correlation and exchange spectra contain the same information about exchange;
(e) the correlation spectrum always has negative cross-peaks;
(f) the sum of the absolute values of the intensities of the cross-peaks can not exceed 50% of the sum of the absolute values of all peaks in the spectrum.

The law (e) lays bare the major fault in the existing ILT-algorithm – conjecture that all the peaks are positive, and makes clear the need to seek for alternatives. The laws established herein can, we believe, be instrumental in such search.

We also analysed the spectra within the perturbation theory as well as the two-site first-order exchange model. These analyses yielded three more features borne by the spectra of the porous systems:

(a) the 50% extremum mentioned in (f) can indeed be achieved;
(b) the correlation spectrum is anti-symmetric with respect to the diagonal and has an equal number of positive and negative cross-peaks;
(c) the signs of the cross-peaks in the correlation spectrum determine thoroughly those in the exchange spectra.

The last two features, though corroborated by several experimental and computer-simulation studies, ought to be viewed as a strong tendency rather than a law. We found that it can have exceptions when relaxation rates assigned to each of the domains of a multi-domain system meet certain conditions.

Acknowledgment

This work was supported by the Agence Nationale de la Recherche (ANR) of France through the ANR-06-JCJC-0106 and ANR-08-ECOT-009 projects.

References

[1] R.R. Ernst, G. Bodenhausen, A. Wokaun, Principles of Nuclear Magnetic Resonance in One and Two Dimensions, Oxford University Press, 1987.
[2] A.E. Derome, Modern NMR Techniques for Chemistry Research, Pergamon Press, 1987.
[3] K. Wüthrich, NMR of Proteins and Nucleic Acids, Wiley, New York, 1986.
[4] R.L. Kleinberg, A. Sezginer, D.D. Griffin, J. Magn. Reson. 97 (1992) 466–485.
[5] G. Eidmann, R. Savelsberg, P. Blümler, B. Blümich, J. Magn. Reson. A 122 (1996) 104–109.
[6] P.S. Aptaker, P.J. McDonald, J. Mitchell, Magn. Reson. Imaging 25 (2007) 548.
[7] A. Abragam, The Principles of Nuclear Magnetism, Clarendon Press, Oxford, 1961.
[8] H.-R. Tang, J. Godward, B. Hills, Carbohydr. Polym. 43 (2000) 375–387.
[9] G. Ovarlez, S. Rodts, A. Ragouilliaux, P. Coussot, J. Goyon, A. Colin, Phys. Rev. E 78 (2008) 036307.
[10] S.V. Dvinskikh, K. Szutkowski, I. Furo, J. Magn. Reson. 198 (2009) 146–150.
[11] R. Blinc, J. Dolinsek, G. Lahajnar, A. Sepe, I. Zupancic, S. Zumer, F. Milia, M.M. Pintar, Z. Naturforsch. A 43 (1988) 1026–1038.
[12] P.F. Faure, S. Rodts, Magn. Reson. Imaging 26 (2008) 1183–1196.
[13] S. Rodts, J. Boujlel, B. Rabideau, G. Ovarlez, N. Roussel, P. Moucheront, C. Lanos, F. Bertrand, P. Coussot, Phys. Rev. E 81 (2010) 021402.

[14] P.J. Prado, B.J. Balcom, S.D. Beyea, T.W. Bremner, R.L. Armstrong, P.E. Grattan-Bellew, Cem. Concr. Res. 28 (1998) 261–270.
[15] J.-P. Korb, M. Whaley-Hodges, R.G. Bryant, Phys. Rev. E 56 (1997) 1934–1945.
[16] S. Stapf, R. Kimmich, R.-O. Seitter, Magn. Reson. Imaging 14 (1996) 841–846.
[17] P.T. Callaghan, Principles of Nuclear Magnetic Resonance Microscopy, Clarendon Press, Oxford, 1993.
[18] A. Plassais, M.-P. Pomiès, N. Lequeux, J.-P. Korb, D. Petit, F. Barberon, B. Bresson, Phys. Rev. E 72 (2005) 041401.
[19] K.P. Whittall, A.L. MacKay, J. Magn. Reson. 84 (1989) 134–152.
[20] S.W. Provencher, Comput. Phys. Commun. 27 (1982) 229–242.
[21] J.P. Butler, J.A. Reeds, S.V. Dawson, SIAM J. Numer. Anal. 18 (1981) 381–397.
[22] J.D. Wilson, J. Mater. Sci. 27 (1992) 3911–3924.
[23] S. Ryu, Magn. Reson. Imaging 19 (2001) 411–415.
[24] B.P. Hills, G. LeFloc'h, Food Chem. 51 (1994) 331–336.
[25] K.R. Brownstein, C.E. Tarr, J. Magn. Reson. 26 (1977) 17–24.
[26] S. Godefroy, J.-P. Korb, M. Fleury, R.G. Bryant, Phys. Rev. E 64 (2001) 021605.
[27] S. Philippot, J.-P. Korb, D. Petit, H. Zanni, Magn. Reson. Imaging 16 (1998) 515–519.
[28] R.L. Kleinberg, S.A. Farooqui, M.A. Horsfield, J. Colloid Interface Sci. 158 (1993) 195–198.
[29] G.C. Borgia, R.J.S. Brown, P. Fantazzini, J. Magn. Reson. 132 (1998) 65–77.
[30] H. Peemoeller, R.K. Shenoy, M.M. Pintar, J. Magn. Reson. 45 (1981) 193–204.
[31] A.E. English, K.P. Whittall, M.L.G. Joy, R.M. Henkelman, Magn. Reson. Med. 22 (1991) 425–434.
[32] J.-H. Lee, C. Labadie, C.S. Springer Jr., G.S. Harbison, J. Am. Chem. Soc. 115 (1993) 7761–7764.
[33] L. Venkataramanan, Y.-Q. Song, M.D. Hürlimann, IEEE Trans. Sig. Process. 50 (2002) 1017–1026.
[34] Y.-Q. Song, L. Venkataramanan, M.D. Hürlimann, M. Flaum, P. Frulla, C. Straley, J. Magn. Reson. 154 (2002) 261–268.
[35] P.J. McDonald, J.-P. Korb, J. Mitchell, L. Monteilhet, Phys. Rev. E 72 (2005) 011409.
[36] T.C. Chandrasekera, J. Mitchell, E.J. Fordham, L.F. Gladden, M.L. Johns, J. Magn. Reson. 194 (2008) 156–161.
[37] P.T. Callaghan, S. Godefroy, B.N. Ryland, Magn. Reson. Imaging 21 (2003) 243–248.
[38] J.G. Seland, K.E. Washburn, H.W. Anthonsen, J. Krane, Phys. Rev. E 70 (2004) 051305.
[39] N. Marigheto, L. Venturi, D. Hibberd, K.M. Wright, G. Ferrante, B.P. Hills, J. Magn. Reson. 187 (2007) 327–342.
[40] R.I. Chelcea, R. Fechete, E. Culea, D.E. Demco, B. Blümich, J. Magn. Reson. 196 (2009) 178–190.
[41] N. Marigheto, L. Venturi, B. Hills, Postharvest Biol. Technol. 48 (2008) 331–340.
[42] Y.-Q. Song, Prog. Nucl. Magn. Reson. Spectrosc. 55 (2009) 324–334.
[43] P.J. McDonald, J. Mitchell, M. Mulheron, L. Monteilhet, J.-P. Korb, Magn. Reson. Imaging 25 (2007) 470–473.
[44] J. Mitchell, M.D. Hürlimann, E.J. Fordham, J. Magn. Reson. 200 (2009) 198–206.
[45] B.P. Hills, S. Benamira, N. Marigheto, K. Wright, Appl. Magn. Reson. 26 (2004) 543–560.
[46] L. Monteilhet, J.-P. Korb, J. Mitchell, P.J. McDonald, Phys. Rev. E 74 (2006) 061404.
[47] K.E. Washburn, P.T. Callaghan, Phys. Rev. Lett. 97 (2006) 175502.
[48] J. Mitchell, J.D. Griffith, J.H.P. Collins, A.J. Sederman, L.F. Gladden, M.L. Johns, J. Chem. Phys. 127 (2007) 234701.
[49] M. Fleury, J. Soualem, J. Colloid Interface Sci. 336 (2009) 250–259.
[50] Y.-Q. Song, L. Zielinski, S. Ryu, Phys. Rev. Lett. 100 (2008) 248002.
[51] S. Rodts, D. Bytchenkoff, J. Magn. Reson. 205 (2010) 315–318.
[52] J.D. Griffith, J. Mitchell, A.E. Bayly, M.L. Johns, J. Phys. Chem. B 113 (2009) 7156–7161.
[53] M. Prange, Y.-Q. Song, J. Magn. Reson. 204 (2010) 118–123.
[54] V. Matveev, D. Bytchenkoff Russ, J. Gen. Chem. 64 (1994) 1435–1438.
[55] T. Kato, Perturbation Theory for Linear Operators, Springer-Verlag, 1976.
[56] E.L. Hahn, Phys. Rev. 76 (1949) 145–147.
[57] H.Y. Carr, E.M. Purcell, Phys. Rev. 94 (1954) 630–638.
[58] S. Meiboom, D. Gill, Rev. Sci. Instrum. 29 (1958) 688–691.
[59] H.C. Torrey, Phys. Rev. 76 (1949) 1059.
[60] I. Solomon, Phys. Rev. Lett. 2 (1959) 301–302.
[61] J.L. Basdevant, J. Dalibard, "Mécanique quantique", Paris, Editions Ellipse, 2001.
[62] S. Ryu, Phys. Rev. E 80 (2009) 026109.
[63] H.M. McConnell, J. Chem. Phys. 28 (1958) 430–431.
[64] J. Crank, The Mathematics of Diffusion, Oxford, New York, 1975.
[65] K.S. Mendelson, Phys. Rev. B 47 (1993) 1081–1083.
[66] B. Sapoval, Th. Gobron, A. Margolina, Phys. Rev. Lett. 67 (1991) 2974–2977.